OPEN ACCESS

KING'S College LONDON

King's Research Portal

DOI:
10.1016/j.actbio.2022.06.032

Document Version
Peer reviewed version

Link to publication record in King's Research Portal

Citation for published version (APA):
Gentleman, E., Merrild, N., Holzmann, V., Ariosa-Morejon, Y., Faull, P. A., Coleman, J., Barrell, W., Young, G., Fischer, R., Kelly, D., Addison, O., Vincent, T., & Grigoriadis, A. (2022). Local depletion of proteoglycans mediates cartilage tissue repair in an ex vivo integration model. *Acta Biomaterialia*, *149*, 179-188. https://doi.org/10.1016/j.actbio.2022.06.032

Citing this paper
Please note that where the full-text provided on King's Research Portal is the Author Accepted Manuscript or Post-Print version this may differ from the final Published version. If citing, it is advised that you check and use the publisher's definitive version for pagination, volume/issue, and date of publication details. And where the final published version is provided on the Research Portal, if citing you are again advised to check the publisher's website for any subsequent corrections.

General rights
Copyright and moral rights for the publications made accessible in the Research Portal are retained by the authors and/or other copyright owners and it is a condition of accessing publications that users recognize and abide by the legal requirements associated with these rights.

•Users may download and print one copy of any publication from the Research Portal for the purpose of private study or research.
•You may not further distribute the material or use it for any profit-making activity or commercial gain
•You may freely distribute the URL identifying the publication in the Research Portal

Take down policy
If you believe that this document breaches copyright please contact librarypure@kcl.ac.uk providing details, and we will remove access to the work immediately and investigate your claim.

Download date: 25. Dec. 2024

Local depletion of proteoglycans mediates cartilage tissue repair in an *ex vivo* integration model

Nicholas Groth Merrild[1], Viktoria Holzmann[1], Yoanna Ariosa-Morejon[2], Peter A. Faull[3], Jennifer Coleman[1], William Barrell[1], Gloria Young[4], Roman Fischer[5], Daniel J. Kelly[6], Owen Addison[7], Tonia L. Vincent[2], Agamemnon E. Grigoriadis[1], Eileen Gentleman[1]*

1. Centre for Craniofacial and Regenerative Biology, King's College London, London, SE1 9RT, UK

2. Centre for OA Pathogenesis Versus Arthritis, Kennedy Institute of Rheumatology, University of Oxford, Oxford, OX3 7FY, UK

3. College of Pharmacy, University of Texas at Austin, Austin, TX 78712, USA

4. Department of Materials, Imperial College London, London, SW7 2AZ, UK

5. Target Discovery Institute, Nuffield Department of Medicine, University of Oxford, Oxford, OX3 7FZ, UK

6. Trinity Centre for Biomedical Engineering, Trinity College Dublin, Dublin, Dublin 2, Ireland

7. Centre for Oral, Clinical & Translational Sciences, King's College London, London, SE1 9RT, UK

*To whom correspondence should be addressed: Eileen Gentleman
Centre for Craniofacial & Regenerative Biology
King's College London
27th Floor, Guy's Hospital
London SE1 9RT UK
eileen.gentleman@kcl.ac.uk
+44 (0) 20 7188 7388

Keywords: *Cartilage repair, proteoglycan depletion, tissue engineering, catabolic enzyme*

Abstract: Successfully replacing damaged cartilage with tissue-engineered constructs requires integration with the host tissue and could benefit from leveraging the native tissue's intrinsic healing capacity; however, efforts are limited by a poor understanding of how cartilage repairs minor defects. Here, we investigated the conditions that foster natural cartilage tissue repair to identify strategies that might be exploited to enhance the integration of engineered/grafted cartilage with host tissue. We damaged porcine articular cartilage explants and using a combination of pulsed SILAC-based proteomics, ultrastructural imaging, and catabolic enzyme blocking strategies reveal that integration of damaged cartilage surfaces is not driven by neo-matrix synthesis, but rather local depletion of proteoglycans. ADAMTS4 expression and activity are upregulated in injured cartilage explants, but integration could be reduced by inhibiting metalloproteinase activity with TIMP3. These observations suggest that catabolic enzyme-mediated proteoglycan depletion likely allows existing collagen fibrils to undergo cross-linking, fibrillogenesis, or entanglement, driving integration. Catabolic enzymes are often considered pathophysiological markers of osteoarthritis. Our findings suggest that damage-induced upregulation of metalloproteinase activity may be a part of a healing response that tips towards tissue destruction under pathological conditions and in osteoarthritis, but could also be harnessed in tissue engineering strategies to mediate repair.

Statement of significance: Cartilage tissue engineering strategies require graft integration with the surrounding tissue; however, how the native tissue repairs minor injuries is poorly understood. We applied pulsed SILAC-based proteomics, ultrastructural imaging, and catabolic enzyme blocking strategies to a porcine cartilage explant model and found that integration of damaged cartilage surfaces is driven by catabolic enzyme-mediated local depletion of proteoglycans. Although catabolic enzymes have been implicated in cartilage destruction in osteoarthritis, our findings suggest that damage-induced upregulation of metalloproteinase activity may be a part of a healing response that tips towards tissue destruction under pathological conditions. They also suggest that this natural cartilage tissue repair process could be harnessed in tissue engineering strategies to enhance the integration of engineered cartilage with host tissue.

1. Introduction

Articular cartilage has a poor capacity to self-heal and damage often progresses to osteoarthritis (OA), a degenerative condition marked by joint pain and loss of cartilage matrix. One therapeutic approach for cartilage repair involves placing either autologous osteochondral grafts or cartilage constructs created using tissue engineering approaches in damaged areas to restore the tissue. However, while grafting can be clinically successful [1], it can also result in unsatisfactory long-term repair [2, 3], an outcome often attributed to a lack of integration between the host and implanted cartilage [4]. Both experimental and *in silico* studies show that poor integration precludes the normal distribution of mechanical forces through cartilage's collagen network [5, 6], thus limiting function. Therefore, the success of cartilage repair strategies may depend on seamlessly integrating grafted/engineered cartilage with the host tissue.

Cartilage is often thought to be incapable of self-repair; however, minor lesions can self-heal [7]. Standard clinical practice is to treat Grade I/II lesions conservatively, and while progression to more serious cartilage damage is common, so too is a lack of progression and even healing. Indeed, in one patient cohort, as many as 37% of asymptomatic lesions identified by MRI improved at follow-up [8]. The repair of damaged matrix in many tissues is mediated by resident/recruited cells that secrete neo-protein. In mice, studies have identified synovial-[9] and superficial zone-resident [10, 11] stem/progenitor cells that can contribute to cartilage repair. However, radiocarbon dating shows that turnover of type II collagen is negligible in human cartilage after skeletal maturity [12], suggesting that neo-collagen synthesis does not contribute to repair in adults. Thus, there is a need to reconcile murine observations of neo-cartilage synthesis with the lack of collagen turnover in humans, and identify mechanisms responsible for cartilage repair.

Type II collagen is abundant in the cartilage ECM, but the tissue also contains large amounts of proteoglycans, which are highly responsive to mechanical cues. For example, joint immobilization drives proteoglycan loss [13]; however, this process is reversible upon remobilization, even to the extent that a highly degraded aggrecan network can be almost completely restored [14]. In diseases

such as OA, degradation of cartilage ECM is mediated by specific matrix metalloproteinases (MMP), including aggrecanases in the A Disintegrin and Metalloproteinase with Thrombospondin Motifs (ADAMTS) family. Under pathological conditions, expression of catabolic enzymes correlates with disease [15]. Thus, MMP13 (which primarily degrades type II collagen) and ADAMTS4/5 (which degrade aggrecan) are considered drivers of OA [16], and murine knockout models of MMP13 [17] and ADAMTS5 [18] both show decreased cartilage degradation in surgically induced models of OA. However, there is emerging evidence that the enzymatic regulation of cartilage is not straightforward as KO models of stromelysin (MMP3) show accelerated development of OA in a joint destabilization model [19]. As catabolic enzymes play diverse and essential roles in tissue repair, these observations suggest that a fresh look at the role of catabolic enzymes in the natural healing of cartilage is warranted.

Here, we used an *ex vivo* porcine explant model of articular cartilage damage to investigate the conditions that foster natural tissue repair to explore strategies that might be exploited to enhance the integration of engineered/grafted cartilage. By visualizing the tissue ultrastructure, performing pulsed SILAC-based proteomics, examining matrix distribution patterns, and inhibiting metalloproteinase activity, we uncover a role for catabolic enzymes in fostering cartilage integration by locally depleting proteoglycans. Our findings suggest that catabolic enzymes may play a reparative role in cartilage by fostering integration of the existing collagen network in response to minor injuries, but under pathological conditions or in OA could tip towards matrix destruction.

2. Materials and Methods

2.1 Preparation of articular cartilage samples for explant culture

8-week-old female pigs (~25kg) were euthanized following the requirements of the Royal Veterinary College Ethics Committee. Femoral condyles were exposed and cartilage (excluding the calcified cartilage layer) were removed from the load-bearing areas of the lateral and medial femoral condyles using a razor blade, and placed in Dulbecco's Modified Eagle's Medium (DMEM). A 6mm diameter biopsy punch was used to cut discs from condylar cartilage, which were placed in chondrogenic

media (DMEM with 4500mg/L glucose supplemented with 10% (v/v) foetal bovine serum (FBS) (Thermo Fisher Scientific), 2mM L-glutamine, 1% (v/v) antibiotic antimycotic (ABAM) (Sigma-Aldrich), and 50µg/mL L-ascorbic acid). Cartilage discs were pre-cultured for 7 days under standard conditions with media changes every 2 days, allowing for lactate dehydrogenase activity to stabilize [20]. For an explanation of sample sizes for experimental assays, see Supplementary Methods.

2.2 Creation of cartilage injury models

2.2.1 "Core/Disc" injury model: After 7 days pre-culture, uninjured control explants (Discs), continued to be cultured in chondrogenic media. To create an injury, a 2mm diameter biopsy punch was used to remove an inner core from the centre of the disc, which was then reinserted, creating a Core/Disc.

2.2.2 "Sheathed Cut" injury model: After 7 days pre-culture, explants were split in half along the vertical axis using a scalpel, separated, realigned, and sheathed within 4mm (internal diameter) sterile polymer tubing that had been split along its vertical axis. The sheath was held in place using sterile dental elastics (ORMCO Zoo Pack Dental Orthodontic Elastics 3.5OZ ¼" Fox Bands). Aggrecanase activity was inhibited in explants by adding 0.5nM TIMP3 (Bio-Techne) in deionized H_20 to culture media.

2.3 Histochemical staining and analysis

Explants were fixed in 4% (w/v) paraformaldehyde (PFA) in PBS on a roller at 4 °C overnight and then washed 3 times in PBS on a roller at room temperature (RT). Samples were dehydrated, embedded in paraffin, and 7µm sections mounted on permafrost slides. Sections from ~1000µm deep into explants were stained. To visualize glycosaminoglycans, sections were stained with Weigert's Iron Haematoxylin, 0.08% (w/v) Fast Green, and 0.1% (w/v) Safranin-O. Collagens were identified by staining with 0.1% (w/v) Picrosirius Red.

Sections were imaged on a Zeiss Apotome using identical microscope settings for all groups. Staining intensity was quantified by converting .TIF images to greyscale. Converted images were either further processed into heat maps or analyzed for whole section or regional intensity levels

surrounding the integration zone using Fiji (version 1.0) by taking mean grey intensity values. To assess integration, sections were processed and stained with Safranin-O, as above. Percent integration was determined by comparing the total length of the integrated line to the total length of the cut surface.

2.4 Immunofluorescence staining for ADAMTS4

7µm explant sections were deparaffinized, rehydrated, and treated with 0.4U/mL Proteinase K (Thermo Fischer Scientific) in PBS for 5 min at RT for antigen retrieval. Sections were then washed 3 times in PBS and treated with blocking solution (BS) composed of 5% (v/v) goat serum in PBS with 0.1% (v/v) Triton™ X-100 (PBST) for 1h at RT. Sections were incubated with anti-ADAMTS4 (1:200, ab185722, Abcam) polyclonal antibody raised in rabbit in BS overnight at 4 °C. Sections were in PBST and incubated with AlexaFluor488-conjugated anti-rabbit IgG (ab150077, Abcam) at 1:250 and Hoechst (1:1000) for 1h at RT. Sections were then washed 3 times in PBST, mounted and imaged on a Leica DMI6000 confocal microscope.

2.5 Freeze/thaw and enzymatically treated samples

After pre-culture, cartilage samples were snap frozen in liquid nitrogen and stored at -80 °C. Control samples were thawed, injured (Sheathed Cut), reassembled, and cultured in chondrogenic media. Enzymatically treated samples were thawed, injured, and enzymatically treated (reported previously [21]) prior to re-assembly and culture in chondrogenic medium or deionized water. For enzymatic treatment, the 2 explant halves were placed together in well plates and treated with gentle agitation at 37 °C in a 5% CO_2 incubator for 24h with 0.6U/mL chondroitinase ABC (Sigma-Aldrich) in 0.05M tris HCL containing 0.06M sodium acetate (pH 8). Explants were then washed in PBS (pH 6) containing 10mM sodium acetate, and then treated for 24h with 20.4 U/mL hyaluronidase from bovine testes (Sigma-Aldrich) with 10mM sodium acetate buffer in PBS (pH 6). Samples were then washed in PBS (pH 7.7) with 1mM $CaCl_2$ and 6mM $MgCl_2$, before being incubated for 3h in 1000 Kunitz U/mL DNase I (Sigma-Aldrich) in PBS (pH 7.7) with 1mM $CaCl_2$ and 6mM $MgCl_2$. Enzymatic treatment steps additionally contained 10mM ethylenediaminetetraacetic acid (EDTA), 1% (v/v)

protease inhibitor cocktail, and 1% ABAM (all from Sigma-Aldrich); however, EDTA was not included in the DNAse I step. Explants were finally washed in PBS, re-assembled and cultured as above.

2.6 Cell viability staining

Thawed cartilage samples and live precultured explants (no freeze-thaw) were placed in PBS with 2µM Calcein AM and 2µM Ethidium Homodimer (Thermo Fischer Scientific) and incubated for 40min before being rinsed in PBS. Samples were then cut in half along their vertical axis, placed cut surface down in well plates and imaged using a Leica DMI6000 confocal microscope.

2.7 Visualization of neo-protein synthesis

After pre-culture, cartilage explants were cultured in L-methionine free media (Life Technologies) with 40µg/mL proline, 2mM L-glutamine, 1mM sodium pyruvate, 0.201mM L-cystine, 50µg/mL L-ascorbic acid, 1% (v/v) ABAM, 10% (v/v) FBS and treated with either 0.1mM L-homopropargylglycine (HPG) (Molecular Probes) or 0.1mM L-methionine (Sigma-Aldrich). Explants were cultured for 7 days (pulse labelling) with media changes every 48h, or for 48h (viability) and fixed in 4% (w/v) PFA. A Click-IT HPG AlexaFluor 488 protein synthesis kit was used to identify HPG (Molecular Probes) in 7µm sections (according to the manufacturer's instruction) and counterstained with 1:1000 Hoechst before imaging on a Leica DMI6000 confocal microscope.

2.8 pSILAC labelling of newly synthesized proteins

Cartilage explants were pre-cultured for 7 days in "light" medium consisting of SILAC DMEM Flex Media without glucose or phenol red (Thermo Fisher Scientific) with 10% (v/v) dialyzed FBS (Thermo Fisher Scientific), 0.1mg/mL L-arginine and 0.1mg/mL L-lysine monohydrochloride. Sheathed Cut or uninjured explants were then placed in "heavy" medium, as above except that L-arginine and L-lysine monohydrochloride were replaced with L-arginine:HCl (13C6, 99%; 15N4, 99%) and L-lysine:2HCl (13C6, 99%; 15N2, 99%) (both from Cambridge Isotope Laboratories). Explants were cultured for 7 days, with media changes every 48h. For details on the methods for protein extraction

and mass spectrometry, liquid chromatography-Tandem Mass Spectrometry (LC-MS/MS), and protein identification, refer to the Supplementary Methods.

2.9 Quantification of ADAMTS4 activity

ADAMTS4 activity was quantified using a Sensolyte 520 Aggrecanase-1 Assay Kit (AnaSpec). This assay is based on a FRET peptide substrate susceptible to cleavable by ADAMTS4. In the intact peptide, the fluorophore 5-FAM is quenched by TAMRA; however, upon cleavage, the fluorescence of 5-FAM is recovered, and its fluorescence can be monitored to quantify ADAMTS4 activity. After pre-culture, uninjured controls and injured explants were cultured in chondrogenic media for 22h. For catabolic enzyme blocking experiments, injured/uninjured explants were cultured with or without 0.5nM TIMP3 treatment for 14 days. Samples were then weighed, the media centrifuged at 1000rcf for 15min at 4 °C, and the supernatant collected. 50µL of substrate solution was combined with 50µL of supernatant, and fluorescence was measured (CLARIOstar Plus, BMG Labtech; 490nm excitation/520nm emission) every 5min for 60min. End-point fluorescence was subtracted from initial fluorescence and divided by cartilage weight to determine activity.

2.10 Scanning electron microscopy

Cartilage explants were dehydrated in 30% (w/v) sucrose (Sigma-Aldrich) in PBS and then infiltrated in Optimal Cutting Temperature (OCT) compound. 30µm cryosections were rinsed and enzymatically treated on an orbital shaker at 37 °C, as above. Sections were washed, fixed in 4% (w/v) PFA in PBS for 20min at RT, washed in PBS, and finally washed in deionized water. Sections were dehydrated in ethanol before the addition of hexamethyldisilazane (Sigma-Aldrich) and air-drying overnight. Glass slides were cut using a diamond blade, mounted on SEM stubs using double-sided carbon tape, and silver painted. Sections were carbon coated (Quorum K975X Carbon Coater) and imaged on a LEO Gemini 1525 FEGSEM.

2.11 Gene expression analyses

Explants (Core/Disc) were snap frozen in liquid nitrogen and stored at -80 °C. Without thawing, explant tissue bases were removed by scalpel, and the edges of the Disc removed using a 4mm

diameter biopsy punch, to isolate the integration area. The remaining 4mm diameter sample was then placed in a mortar pre-cooled with liquid nitrogen and ground with a pestle. RLT Buffer (Qiagen) with 10µL/mL β-mercaptoethanol (Sigma-Aldrich) was added and the solution vortexed for 20s and centrifuged at 12,000rcf for 1h at 4 °C. RNA was extracted using an RNeasy kit (Qiagen). qPCR performed on a LightCycler® 480 Instrument II (Roche). The reaction mixture consisted of 2ng of cDNA, 250nM of primers, and 5µL 2X Brilliant III SYBR® Green Mastermix (Agilent Technologies). The ΔΔCT method was used to calculate fold change expression. Primer sequences (Supplementary Table 1, Integrated DNA Technologies) were designed using Primer3 and BLAST.

2.12 Mechanical testing to determine integration strength

Tensile tests were performed on Sheathed Cut explants using an Instron 5569A with a 500N load cell. Explants were oriented on a glass slide with the integration axis perpendicular to the axis of tension and glued (Super Glue Gel, Gorilla) to the slide with activator (Loctite SF 7457, Henkel Adhesives). The glass slide holding the explant was then secured to the lower platen with double-sided tape (Heavy Duty Mounting Tape, Gorilla). A glass slide was similarly affixed to the upper platen, brought into contact with the cartilage sample and glued. A tensile test was then performed at a strain of 1mm/min and peak force (N) recorded at tensile failure. All samples failed at the interface.

To determine contact area, broken explants were fixed in 4% (w/v) PFA, washed in PBS and stored in 70% IMS at 4 °C. Explants were placed integration side down on glass slides and imaged in a Zeiss Apotome microscope. Total contact surface area was measured in FIJI and failure stress (kPa) calculated by dividing peak force by the contact surface area.

2.13 Statistical analyses

Data are presented as means and standard deviations. Multiple comparisons were carried out using a One-way ANOVA followed by a post-hoc Tukey test. Comparisons between two groups were performed using an unpaired two-tailed t-test. All analyses were performed using GraphPad Prism 8 for Windows.

3. Results

3.1 Juvenile porcine articular cartilage self-repairs in an *ex vivo* culture model

To establish a model of cartilage repair in response to injury, we modified van Osch *et al*.'s protocol whereby a circular defect (core) created in juvenile porcine knee articular cartilage (disc) integrates upon *ex vivo* culture [22, 23]. However, in this established "Core/Disc" model, the core can sometime slip within the disc, resulting in areas that integrate poorly. Therefore, we also developed an alternative approach in which damaged cartilage surfaces were mechanically held together ("Sheathed Cut") (Fig. 1a). Using both these models, we were able to replicate the reported integration of cartilage, with near seamless integration by 28 days in culture, as shown in Safranin-O and type II collagen-stained sections (Fig. 1b/c and Supplementary Fig. 1). Scanning electron microscopy (SEM) imaging of explants revealed fibrils spanning the integration zone (Fig. 1d and Supplementary Fig. 2). These observations confirm that damaged juvenile porcine cartilage explants integrate across cut surfaces during *ex vivo* culture, creating areas in which a continuous fibrous network spans the defect.

3.2 Neo-protein synthesis in the integration zone is not accompanied by increased expression of cartilage transcription factors, key matrix proteins or cross-linking enzymes

To better understand the processes that were driving tissue integration in our *ex vivo* model, we first used a non-canonical amino acid labelling technique (FUNCAT) to visualize neo-protein production (Fig. 1e). In keeping with previous reports that sharp injuries do not cause extensive cell death [24], confocal images of sections through the defect after 7 days of culture showed strong signal in chondrocytes, indicative of live cells. However, we also observed signal along the integration surface (Fig. 1f). We first hypothesized that integration was driven by resident chondrocytes upregulating genes required for the formation of articular cartilage during development. However, we could not detect regulation of genes encoding for types I, II, or X collagen, or the transcription factor Sox9 (Supplementary Fig. 3). In murine models, Gdf5-lineage cells have been shown to populate an injury site [9]. However, we never observed nuclei concentrated along the cut tissue surfaces, nor did we

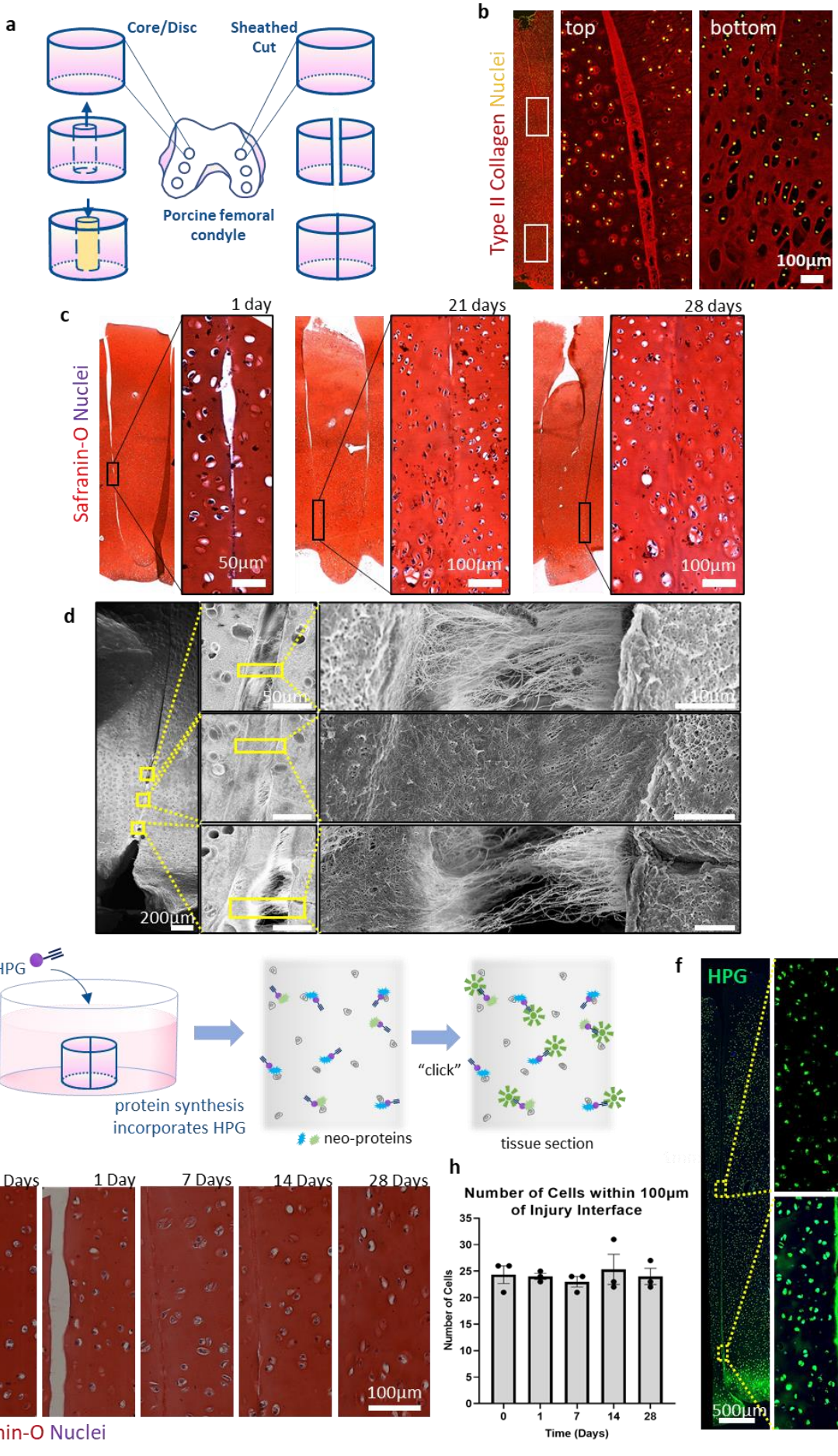
a
Core/Disc
Sheathed Cut
Porcine femoral condyle
b
Type II Collagen Nuclei
top
bottom
100µm
c
1 day
21 days
28 days
Safranin-O Nuclei
50µm
100µm
100µm
d
50µm
10µm
200µm
e
HPG
protein synthesis incorporates HPG
neo-proteins
"click"
tissue section
f
HPG
100µm
500µm
g
0 Days
1 Day
7 Days
14 Days
28 Days
100µm
Safranin-O Nuclei
h
Number of Cells within 100µm of Injury Interface
Number of Cells
Time (Days)
0
1
7
14
28

Figure 1: a) Schematic illustrating injury models on porcine cartilage explants. A biopsy punch is used to extract discs from porcine femoral condyle cartilage. Cartilage is then injured by punching out and replacing a smaller core, creating the "Core/Disc" model, or is cut down the centre and then placed in a cylindrical polymer sheath held together with a dental elastic, creating a "Sheathed Cut". **b)** Representative low and high magnification confocal images along cut surface showing immunostaining for type II collagen in a Core/Disc model after 28 days in culture. Some areas show seamless integration (n=3 explants, from pool collected from 10 pigs). **c)** Time course of Safranin-O staining of paraffin sections from Core/Disc model. After 21 and 28 days in culture, cartilage surfaces in close contact show apparently seamless integration (n=3 explants, from pool collected from 10 pigs). **d)** Representative scanning electron microscopy images across the defect of a Sheathed Cut explant after 28 days in culture. Integrated areas show fibrils spanning the defect. In some areas, what appear to be previously integrated areas have been pulled apart (likely as an artefact of the sample preparation process), revealing the fibrous network (n=3 explants, from pool collected from 5 pigs). **e)** Schematic illustrating the non-canonical amino acid tagging technique (FUNCAT) whereby the non-canonical amino acid L-homopropargylglycine (HPG) placed in explant culture media is incorporated into newly synthesized proteins and then detected in tissue sections via a "click" reaction that attaches a fluorophore. **f)** Representative confocal images of a Core/Disc section after a 7 day "pulse" to label newly synthesized proteins. Positive signal is evident within cells and concentrated at the cut surfaces (n=2 explants from 2 pigs). **g)** Representative Safranin-O stained sections from Sheathed Cut explants over 28 days in culture (n=3 explants, from pool collected from 4 pigs). **h)** Quantification of the number of cells visible within 100µm of the interface in Sheathed Cut samples (n=3 explants, from pool collected from 4 pigs). The number of cells near the interface does not change over time in culture ($p>0.05$; One-way ANOVA with Tukey test).

see evidence of migration of resident chondrocytes (Fig. 1g). Indeed, quantification of cell number at the integration zone showed that it was no different from that in the bulk tissue (Fig. 1h).

We next hypothesized that integration could have been mediated by upregulation of genes encoding enzymatic cross-linkers of the existing collagen network. However, we could detect no changes in the expression levels of lysyl oxidase (LOX) or any of its isoforms (Supplementary Fig. 4). These observations suggest that although neo-protein accumulates near the cut surfaces, this is not accompanied by recruitment of cells nor upregulation of markers associated with cartilage development or the enzymatic cross-linking of collagen.

3.3 Articular cartilage spontaneously integrates in the absence of live cells when proteoglycans are depleted

Previous reports have suggested that integration of cut surfaces was enhanced in explants in which proteoglycans were depleted from the wound edges, particularly if they were also treated with collagenase. This phenomenon has been correlatively linked to increased cell densities near the

integration zone [25]. Our model foregoes collagenase digestion, which likely precludes migration, thus accounting for the lack of differential cell accumulation in the integration zone. Therefore, as we observed integration in the absence of cell accumulation, we next asked if integration was possible in the absence of live cells, and if it could be enhanced by locally depleting proteoglycans.

To test this, we devitalized cartilage explants by freeze-thaw, enzymatically treated them and then cultured them *ex vivo*. Live-dead staining confirmed a complete absence of viable cells in explants subjected to freeze-thaw (Fig. 2a), which we confirmed by FUNCAT (Supplementary Fig. 5). Safranin-O staining of paraffin-sectioned explants showed that non-enzymatically treated samples showed limited integration, but that enzymatically treated samples showed good integration (Fig. 2b), similar to that in living tissues samples (Fig. 1b). SEM imaging across the cut surface of enzymatically treated devitalized samples similarly revealed that in integrated areas, a continuous fibrous network spanned the formerly severed region (Fig. 2c). In these devitalized samples, neo-protein synthesis could not have driven integration; however, to rule out the possibility that serum proteins accumulated along the integration zone, we also cultured explants in deionized water, and again identified a continuous network spanning the defect (Supplementary Fig. 6). Moreover, when we performed tensile tests to assess the strength of the integration, we found that while non-enzymatically treated samples were similar to uncultured controls, the failure stress for enzymatically treated explants both cultured in medium and deionized water was higher than either untreated or uncultured controls (Fig. 2d). Taken together, these observations suggest that collagen re-assembles across cut juvenile porcine cartilage surfaces in the absence of neo-matrix synthesis when proteoglycans are depleted from the integration zone.

3.4 pSILAC labelling shows negligible neo-cartilage matrix formation in response to injury

To better understand how our observations of integration in enzymatically treated, devitalized explants related to integration in living explant cultures, we performed a “pulse” stable isotope labelling by amino acids in cell culture (pSILAC) experiment. We cultured both injured and uninjured explants in medium containing heavy isotope labelled arginine(10) and lysine(8), which are

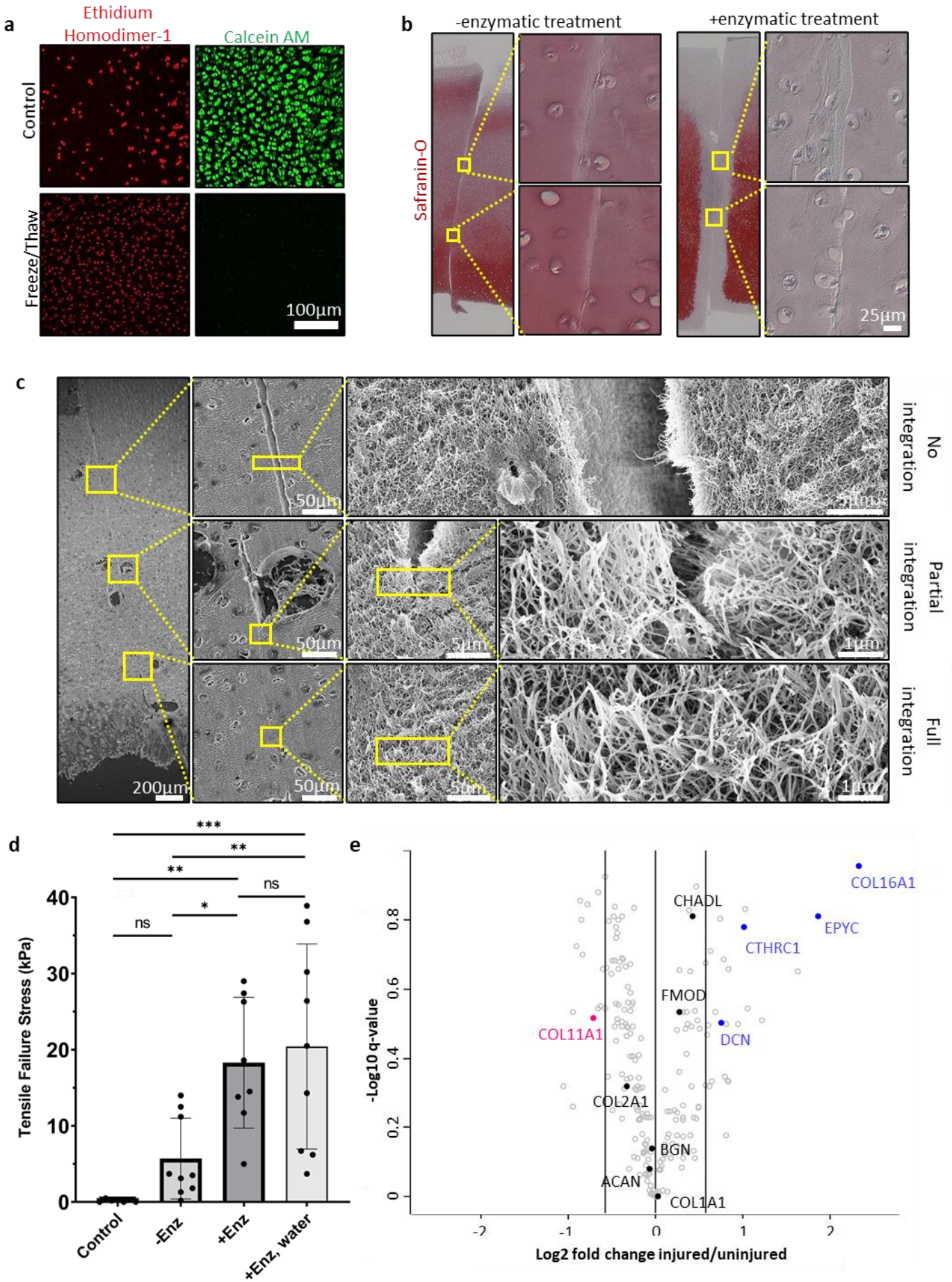
a
Ethidium Homodimer-1
Calcein AM
Control
Freeze/Thaw
100µm
b
-enzymatic treatment
+enzymatic treatment
Safranin-O
25µm
c
No integration
Partial integration
Full integration
200µm
50µm
5µm
1µm
d
Tensile Failure Stress (kPa)
Control
-Enz
+Enz
+Enz, water
***
**
**
*
ns
ns
e
-Log10 q-value
Log2 fold change injured/uninjured
COL16A1
CHADL
EPYC
CTHRC1
FMOD
COL11A1
DCN
COL2A1
BGN
ACAN
COL1A1

Figure 2: a) Representative Live/Dead fluorescence images of porcine cartilage explants either cultured as normal or subjected to a single freeze/thaw cycle after 7 days in culture (n=2 explants, from pool collected from 6 pigs). **b)** Safranin-O staining of Sheathed Cut explants after 1 freeze/thaw cycle, with or without enzymatic treatment (chondroitinase ABC+hyaluronidase) and cultured for 23 days (n=4 explants, from pool collected from 4 pigs). **c)** Representative scanning electron microscopy images across the defect of a Sheathed Cut explant after 1 freeze/thaw cycle and enzymatic treatment after 23 days in culture. Integrated areas show fibrils spanning the defect (n=4 explants, from pool collected from 4 pigs). **d)** Ultimate failure stress of Sheathed Cut cartilage explants after 1 freeze/thaw cycle, with or without enzymatic treatment (Enz-/+), and cultured for 14 days in culture medium or deionized water (n>7 explants, from pool collected from 12 pigs; One-way ANOVA with Tukey test, *p<0.05, **p<0.01, ***p<0.001). **e)** Volcano plot from pSILAC-based proteomics analyses of Sheathed Cut explants (n=4 explants, from pool collected from 6 pigs). Blue dots highlight matrix proteins that were more than 50% upregulated in the injured group. Pink dots identify proteins that were more than 50% downregulated in the uninjured controls. No protein had a -log q-value>1 (q<0.1).

metabolically incorporated into newly synthesized proteins (Supplementary Fig. 7). Using mass spectrometry, we identified 211 proteins for which we could calculate heavy/light ratios in all biological replicates (Supplementary Dataset 1). No protein had an adjusted *p*-value (*q*) less than 0.1 when comparing heavy/light ratios in injured versus uninjured explants. Analysis of the major protein constituents of cartilage revealed an overall lack of regulation in response to injury with a *q*-value of type II collagen of 0.47, aggrecan *q*=0.83, decorin *q*=0.31, biglycan *q*=0.73 and fibromodulin *q*=0.29. Similarly, other fibril forming minor collagens like type XI, were not regulated (*q*=0.31) (Fig. 2e). Of the secreted matrix proteins that had *q* values <0.2, we identified collagen triple helix repeat containing 1 (CTHRC1), epiphycan (EPYC), chondroadherin-like (CHADL) and type XVI collagen (COL16A1), which were all upregulated in response to injury. CTHRC1 is involved in vascular remodelling, and its levels are elevated in the plasma of patients with rheumatoid arthritis [26]. CHADL modulates collagen fibrillogenesis and chondrocyte differentiation, and plays a role in the formation of a stable cartilage ECM [27]. Epiphycan (like other small leucine rich proteoglycans in cartilage) and COL16A1 are both recognized to stabilize collagen fibrils [28, 29].

3.5 Catabolic enzymes that locally deplete proteoglycans improve integration strength

pSILAC labelling revealed no differential neo-synthesis of the main proteinaceous constituents of native cartilage in response to injury, and instead only highlighted subtle regulation of proteins known to stabilize the cartilage matrix. Moreover, as we had observed that integration was limited in devitalized samples that had not been enzymatically treated, we next hypothesized that the positive

staining along the integration zone in our metabolic labelling experiment (Fig. 1f) had identified a catabolic enzyme that was playing a role in fostering integration in our living samples by depleting proteoglycans. In line with previous reports that matrix catabolic enzymes are rarely detected using proteomics [30], we did not identify metalloproteinases in our samples by mass spectrometry (Supplementary Dataset 1). ADAMTS5 plays a central role in cartilage degradation in mouse [18]; however, in humans both ADAMTS4 and ADAMTS5 have been implicated [31]. As tools available for use in pig better suite analysis of ADAMTS4, we first performed qPCR and found that expression was higher 2h after tissue injury compared to uninjured controls (Fig. 3a). This is in keeping with previous reports of upregulation of ADAMTS4 in a mini-pig model upon induction of post-traumatic OA [32]. Our observation of increased ADAMTS4 expression was confirmed by immunostaining, which showed increased intensity locally at the cut surfaces 24h after injury (Fig. 3b and Supplementary Fig. 8). Immunostaining confirmed that that type II collagen was ubiquitous across the integration zone, while type I collagen was undetectable (Supplementary Fig. 9). Quantification of staining for collagens by Sirius red showed neither bulk nor local decreases in staining near the integration zone (Fig. 3c). However, positive staining for ADAMTS4 correlated with decreased local staining for proteoglycans by Safranin-O at 1 and 7 days post-injury, compared to the bulk tissue (Fig. 3d and Supplementary Fig. 10). The ability of ADAMTS4 to act at sites distant from resident cells is supported by previous reports of positive staining for epitopes cleaved by aggrecanases in the interterritorial matrix [33]. In line with reports that proteoglycans are degraded in unloaded tissues [13], we similarly saw a reduction in total staining by day 28 (Supplementary Fig. 11).

To further link proteoglycan depletion to integration, we next used a commercial FRET-based assay (Sensolyte® 520 Aggrecanase-1 Assay Kit, AnaSpec) to confirm that injured cartilage showed increased ADAMTS4 activity compared to uninjured (Fig. 3e), and that this activity could be reduced by culturing injured explants with tissue inhibitor of metalloproteinase 3 (TIMP3) (Fig. 3f), which strongly inhibits the activity of ADAMTS4 and other metalloproteinases. TIMP3 inhibition reduced the total integration area of cultured explants (Fig. 3g), and preserved Safranin-O staining intensity in the integration area (Fig. 3h). It also resulted in decreased failure stress compared to untreated controls (Fig. 3i). These data show that local proteoglycan depletion, which correlates with increased

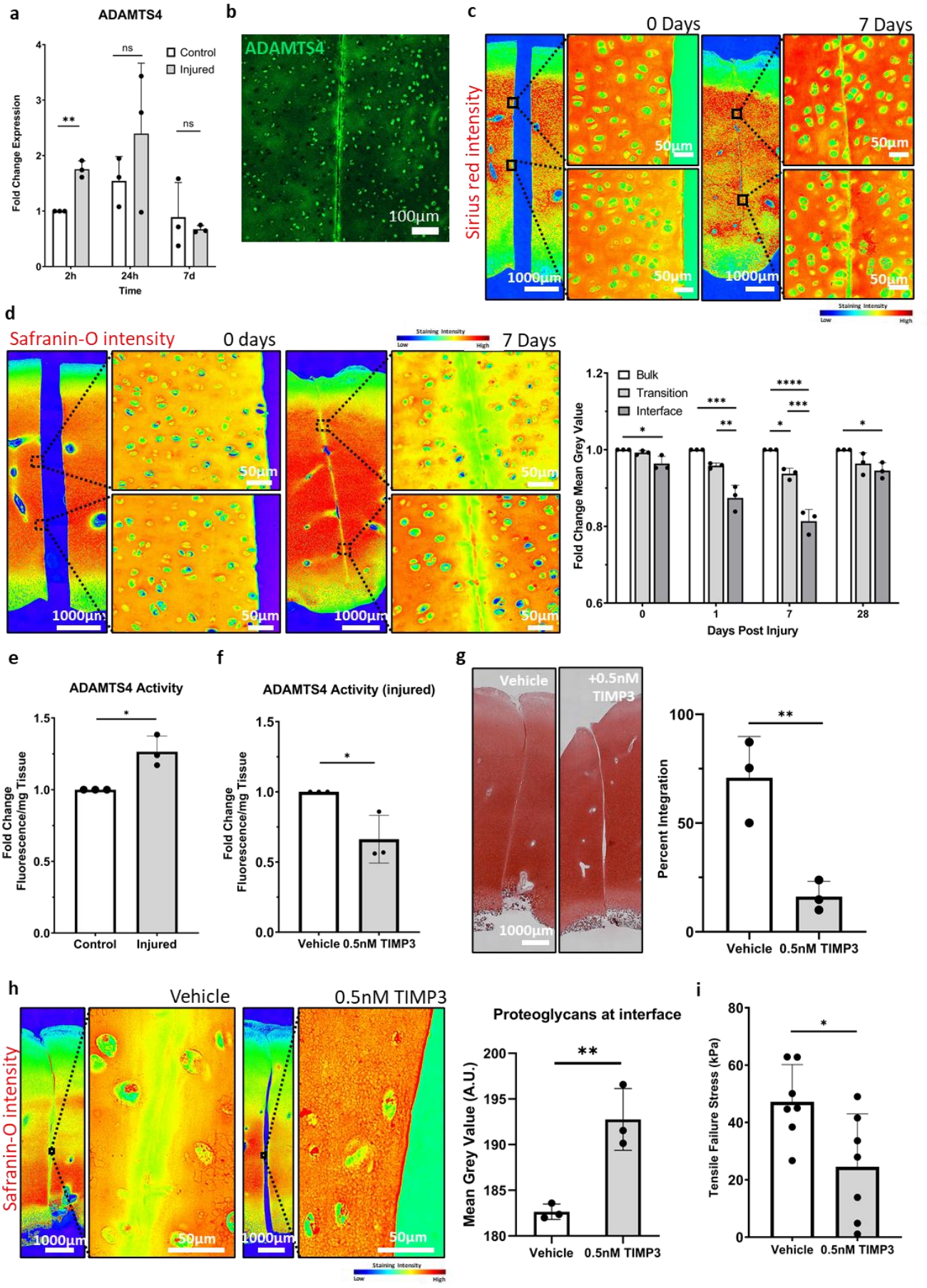
a
ADAMTS4
Fold Change Expression
Control
Injured
ns
**
ns
2h
24h
7d
Time
b
ADAMTS4
100µm
c
0 Days
7 Days
Sirius red intensity
50µm
1000µm
Staining Intensity
Low
High
d
Safranin-O intensity
0 days
7 Days
Bulk
Transition
Interface
Fold Change Mean Grey Value
Days Post Injury
e
ADAMTS4 Activity
Fold Change Fluorescence/mg Tissue
Control
Injured
f
ADAMTS4 Activity (injured)
Vehicle
0.5nM TIMP3
g
Vehicle
+0.5nM TIMP3
Percent Integration
h
Vehicle
0.5nM TIMP3
Safranin-O intensity
Proteoglycans at interface
Mean Grey Value (A.U.)
i
Tensile Failure Stress (kPa)

Figure 3: a) Fold change ADAMTS4 expression in Core/Disc explants 2h, 24h and 7 days after injury (n=3 explants, from pool collected from 9 pigs). **b)** Representative confocal image showing immunostaining for ADAMTS4 along the cut surfaces of a Core/Disc explant 24h after injury (n=3 explants, from pool collected from 10 pigs). **c)** Representative false color Sirius Red staining intensity images for Sheathed Cut explants cultured for 0 or 7 days (n=3 explants, from pool collected from 4 pigs). **d)** Representative false color Safranin-O staining intensity images for Sheathed Cut explants cultured for 0 or 7 days with corresponding quantification of intensity in the integration, transition, and bulk of sections (n=3 explants, from pool collected from 4 pigs; One-way ANOVA with Tukey test, *p<0.05, **p<0.01, ***p<0.001, ****p<0.0001). **e)** Quantification of ADAMTS4 activity in uninjured and Sheathed Cut explants 22h after injury (n=3 explants from 3 pigs, unpaired t-test, two-tailed *p<0.05). **f)** Biochemical quantification of ADAMTS4 activity in Sheathed Cut explants 22h after injury treated with either 0.5nM TIMP3 or vehicle (n=3 explants from 3 pigs, unpaired t-test, two-tailed, *p<0.05). **g)** Representative Safranin-O staining of Sheathed Cut explants cultured for 14 days either under standard conditions or supplemented with 0.5nM TIMP3. Quantification shows the percent of the total surface that was integrated (n=3 explants, from pool collected from 6 pigs; unpaired t-test, two-tailed, **p<0.01). **h)** Representative false color Safranin-O staining intensity images for Sheathed Cut explants cultured for 14 days with vehicle or 0.5nM TIMP3 with corresponding quantification of intensity in the integration area (n=3 explants, from pool collected from 6 pigs; unpaired, two-tailed t-test). **i)** Ultimate failure stress of Sheathed Cut cartilage explants cultured for 14 days under standard conditions (vehicle) or treated with 0.5nM TIMP3 (n=7 explants, from pool collected from 6 pigs; unpaired t-test, two-tailed, *p<0.05).

ADAMTS4 activity, allows for cartilage tissue integration, and that inhibition of catabolic enzyme activity with TIMP3 preserves proteoglycans in the integration zone and reduces integration.

4. Discussion

Here we used a porcine explant model of cartilage tissue damage to identify drivers of natural cartilage repair that might be harnessed to improve integration between engineered/grafted cartilage constructs and native tissue. In line with previous reports [22, 23, 25], we show that cut juvenile porcine cartilage can assemble a fibrous network that spans the defect. However, integration did not appear to be driven by cell accumulation nor neo-cartilage matrix synthesis in the integration zone, and although we observed neo-proteins at the interface, this was not required for integration. Instead, we found that devitalized tissue integrated if depleted of proteoglycans, suggesting a catabolic enzyme-driven process. We then analyzed tissues for ADAMTS4 and found that its expression and activity were upregulated in injured tissues and concentrated at the defect site. We also found that inhibition of catabolic enzymes with TIMP3 preserved proteoglycans in the integration zone, reduced tissue integration, and reduced the stress required to rupture the integrated surfaces. Although our

analyses only correlate ADAMTS4 activity with integration and cannot rule out a role for other catabolic enzymes (ADAMTS5, MMP13, *e.g.*), taken together, they implicate local proteoglycan depletion as a mediator of integration of the existing collagenous network in the absence of neo-matrix synthesis (Supplementary Fig. 12).

Murine models of cartilage damage have identified migratory populations that contribute to healing [9]. Failure of cell migration is thought to limit articular cartilage repair and previous observations of integration in bovine tissue models after enzymatic treatment have often been attributed to cell migration [34, 35]. However, our findings suggest that a cell migration-independent, enzyme-driven process might act independently or alongside cell-driven processes, contributing to repair. This integration process did not require new collagenous ECM deposition, as devitalized tissues also repaired, and we could not detect differential heavy pSILAC label in any of the major proteinaceous constituents of cartilage.

LOX enzymes are critical in establishing cartilage's collagen network. Exogenous treatment with LOX improves the tensile strength of native and TE cartilage [36], and enhances integration with native tissue explants [37]. We found no regulation of LOX or any of the isoforms in our cultures, suggesting limited availability at the cut surfaces. Although these observations do not rule out a role for LOX-mediated cross-linking of the collagen network, as resident enzymes in the tissue could have contributed to repair, they are in keeping with a lack of regulation of LOX expression in acute damage models [32, 38]. However, collagen is also known to undergo other assembly processes, often in the absence of neo-matrix production, to establish and strengthen its network. For example, collagen can form advanced glycation end-products between free amino acid residues and reducing sugars, but in our devitalized cultures in deionized water, such processes are unlikely. However, collagen also undergoes fibrillogenesis, a process that is known to be limited when highly negatively charged proteoglycans are bound to collagen fibrils. This has led some to suggest that one role of proteoglycans (and small leucine rich proteoglycans, in particular) is to sterically prevent the uncontrolled assembly of collagens into fibers [39]. In *in vitro* models, the presence of aggrecan slows collagen fibrillogenesis [40]. Lubricin null mice experience extensive collagen fibrillation on the

cartilage surface [41], and in the cartilage of decorin null mice, injury, which depletes the tissue of aggrecan, similarly leads to extensive collagen fibrillation [42]. Thus, we speculate that enzymatically driven loss of proteoglycans in our model could foster collagen entanglement, fibrillation, and/or non-enzymatic cross-linking of the existing collagen network, driving integration. Indeed, if one imagines how Velcro functions by adhering when pushed together, a similar process in damaged cartilage surfaces could also explain the range of failure stresses we observed in our tensile tests. Our injury did not control for collagen orientation, which varies in the superficial, middle and deep zones of the tissue. Thus, damaged surfaces created by cutting fibrils perpendicular or parallel to the native collagen orientation could have rendered them more or less likely to interact when placed together. Moreover, the strength of the repaired tissue remained orders of magnitude lower than that of uninjured cartilage, suggesting more robust processes would be required to ensure a functional repair.

Depletion of proteoglycans precedes collagen degradation as an early sign of OA [43] and ADAMTS4/5 and MMP3/13 (among others) have been implicated in cartilage destruction in OA. As a result, small molecule inhibitors and nanobodies against catabolic enzymes are being enthusiastically pursued as OA treatments [44, 45]. However, our observations that local depletion of proteoglycans improves integration, opens the possibility that local matrix catabolism and the dynamic turnover of the proteoglycan network in response to injury may in fact be part of an intrinsic process that repairs minor defects by facilitating integration of the existing collagen network. However, upon severe damage, the continued expression of catabolic enzymes results in pathological degradation of the tissue. As these enzymes are evolutionarily conserved in vertebrates [46], our proposal of a healing role is in keeping with the generally accepted notion that a predominantly deleterious function would not be maintained.

Researchers have tried to foster integration between engineered constructs and native cartilage using growth factors as chemoattracts [47] and adhesive strategies [48, 49]. Enzymatic digestion of tissues/constructs, including their collagenous network has also been attempted [50]. Indeed, several reports suggest that enzymatic treatment fosters graft integration; however, this has often

been attributed to increased cell migration and neo-matrix synthesis [50, 51]. Our observations instead suggest that tissue engineering strategies might additionally benefit from targeted approaches that selectively deplete the proteoglycan network alone at tissue/construct edges and a period of unloading post implantation. Together, these strategies may allow researchers to harness the tissue's intrinsic ability to foster integration of the collagenous network.

5. Conclusions

We demonstrate that locally depleting proteoglycans improves tissue integration in an articular cartilage explant model. These findings reframe our current understanding of catabolic enzymes as principally pathophysiological mediators in the joint. Our data shed light on mechanisms of intrinsic cartilage repair and suggest that autologous grafting and tissue engineering strategies may benefit from locally depleting the proteoglycan network to improve the integration of constructs.

6. Acknowledgements

We are grateful for support from Dermot Daly of Trinity College Dublin and the Advanced Microscopy Laboratory, Graham Haggar of the Royal Veterinary College, and Mahmoud Ardakani at Imperial College London Department of Materials for assistance with electron microscopy.

7. Author contributions

NGM, AEG and EG conceptualized the study. NGM, VH, JC, WB, YA-M, RF and GY performed experiments. NGM, PAF and YA-M carried out data analysis. OA, TV, RF, DJK, AEG and EG supervised the work. NGM and EG wrote and edited the manuscript. All authors approved the manuscript.

8. Role of funding source

This study was supported by the UK Medical Research Council (MRC) Doctoral Training Partnership in Biomedical Sciences at King's College London (award to NGM) and the MRC Flexible Supplement Fund. The funder played no role in the design of analysis of the data in this study.

9. Conflict of Interest

The authors declare no competing interests.

10. Data and materials availability

The mass spectrometry proteomics data have been deposited to the ProteomeXchange Consortium via the PRIDE [52] partner repository with the dataset identifier xxxx. Reviewer account details are as follows**:** Username: xxxx Password: xxxxx. All other data are available in the main text or the supplementary materials.

11. References

[1] E. Solheim, J. Hegna, T. Strand, T. Harlem, E. Inderhaug, Randomized Study of Long-term (15-17 Years) Outcome After Microfracture Versus Mosaicplasty in Knee Articular Cartilage Defects, Am J Sports Med 46(4) (2018) 826-831.
[2] G. Filardo, E. Kon, F. Perdisa, C. Tetta, A. Di Martino, M. Marcacci, Arthroscopic mosaicplasty: long-term outcome and joint degeneration progression, Knee 22(1) (2015) 36-40.
[3] E. Solheim, J. Hegna, E. Inderhaug, Long-Term Survival after Microfracture and Mosaicplasty for Knee Articular Cartilage Repair: A Comparative Study Between Two Treatments Cohorts, Cartilage 11(1) (2020) 71-76.
[4] M. Marcacci, E. Kon, M. Delcogliano, G. Filardo, M. Busacca, S. Zaffagnini, Arthroscopic autologous osteochondral grafting for cartilage defects of the knee: prospective study results at a minimum 7-year follow-up, Am J Sports Med 35(12) (2007) 2014-21.
[5] S.L. Bevill, A. Thambyah, N.D. Broom, New insights into the role of the superficial tangential zone in influencing the microstructural response of articular cartilage to compression, Osteoarthritis Cartilage 18(10) (2010) 1310-8.
[6] S.M. Hosseini, Y. Wu, K. Ito, C.C. van Donkelaar, The importance of superficial collagen fibrils for the function of articular cartilage, Biomech Model Mechanobiol 13(1) (2014) 41-51.
[7] F. Dell'accio, T.L. Vincent, Joint surface defects: clinical course and cellular response in spontaneous and experimental lesions, Eur Cell Mater 20 (2010) 210-7.
[8] C. Ding, F. Cicuttini, F. Scott, H. Cooley, C. Boon, G. Jones, Natural history of knee cartilage defects and factors affecting change, Arch Intern Med 166(6) (2006) 651-8.
[9] A.J. Roelofs, J. Zupan, A.H.K. Riemen, K. Kania, S. Ansboro, N. White, S.M. Clark, C. De Bari, Joint morphogenetic cells in the adult mammalian synovium, Nat Commun 8 (2017) 15040.
[10] E. Kozhemyakina, M. Zhang, A. Ionescu, U.M. Ayturk, N. Ono, A. Kobayashi, H. Kronenberg, M.L. Warman, A.B. Lassar, Identification of a Prg4-expressing articular cartilage progenitor cell population in mice, Arthritis Rheumatol 67(5) (2015) 1261-73.
[11] L. Li, P.T. Newton, T. Bouderlique, M. Sejnohova, T. Zikmund, E. Kozhemyakina, M. Xie, J. Krivanek, J. Kaiser, H. Qian, V. Dyachuk, A.B. Lassar, M.L. Warman, B. Barenius, I. Adameyko, A.S. Chagin, Superficial cells are self-renewing chondrocyte progenitors, which form the articular cartilage in juvenile mice, FASEB J 31(3) (2017) 1067-1084.
[12] K.M. Heinemeier, P. Schjerling, J. Heinemeier, M.B. Moller, M.R. Krogsgaard, T. Grum-Schwensen, M.M. Petersen, M. Kjaer, Radiocarbon dating reveals minimal collagen turnover in both healthy and osteoarthritic human cartilage, Sci Transl Med 8(346) (2016) 346ra90.
[13] M. Nomura, N. Sakitani, H. Iwasawa, Y. Kohara, S. Takano, Y. Wakimoto, H. Kuroki, H. Moriyama, Thinning of articular cartilage after joint unloading or immobilization. An experimental investigation of the pathogenesis in mice, Osteoarthritis Cartilage 25(5) (2017) 727-736.
[14] M.A. Karsdal, S.H. Madsen, C. Christiansen, K. Henriksen, A.J. Fosang, B.C. Sondergaard, Cartilage degradation is fully reversible in the presence of aggrecanase but not matrix metalloproteinase activity, Arthritis Res Ther 10(3) (2008) R63.
[15] L. Kevorkian, D.A. Young, C. Darrah, S.T. Donell, L. Shepstone, S. Porter, S.M. Brockbank, D.R. Edwards, A.E. Parker, I.M. Clark, Expression profiling of metalloproteinases and their inhibitors in cartilage, Arthritis Rheum 50(1) (2004) 131-41.
[16] H. Nagase, M. Kashiwagi, Aggrecanases and cartilage matrix degradation, Arthritis Res Ther 5(2) (2003) 94-103.
[17] C.B. Little, A. Barai, D. Burkhardt, S.M. Smith, A.J. Fosang, Z. Werb, M. Shah, E.W. Thompson, Matrix metalloproteinase 13-deficient mice are resistant to osteoarthritic cartilage erosion but not chondrocyte hypertrophy or osteophyte development, Arthritis Rheum 60(12) (2009) 3723-33.
[18] S.S. Glasson, R. Askew, B. Sheppard, B. Carito, T. Blanchet, H.L. Ma, C.R. Flannery, D. Peluso, K. Kanki, Z. Yang, M.K. Majumdar, E.A. Morris, Deletion of active ADAMTS5 prevents cartilage degradation in a murine model of osteoarthritis, Nature 434(7033) (2005) 644-8.
[19] K.M. Clements, J.S. Price, M.G. Chambers, D.M. Visco, A.R. Poole, R.M. Mason, Gene deletion of either interleukin-1beta, interleukin-1beta-converting enzyme, inducible nitric oxide synthase, or stromelysin 1

accelerates the development of knee osteoarthritis in mice after surgical transection of the medial collateral ligament and partial medial meniscectomy, Arthritis Rheum 48(12) (2003) 3452-63.
[20] M. de Vries-van Melle, E. Mandl, N. Kps, W. Koevoet, J. Verhear, G. van Osch, An Osteochondral Culture Model To Study Mechanisms Involved in Articular Cartilage Repair, Tissue Engineering Part C - Methods.
[21] W.S. Vanden Berg-Foels, L. Scipioni, C. Huynh, X. Wen, Helium ion microscopy for high-resolution visualization of the articular cartilage collagen network, J Microsc 246(2) (2012) 168-76.
[22] L.M. Janssen, C.D. In der Maur, P.K. Bos, J.A. Hardillo, G.J. van Osch, Short-duration enzymatic treatment promotes integration of a cartilage graft in a defect, Ann Otol Rhinol Laryngol 115(6) (2006) 461-8.
[23] J. van de Breevaart Bravenboer, C.D. In der Maur, P.K. Bos, L. Feenstra, J.A. Verhaar, H. Weinans, G.J. van Osch, Improved cartilage integration and interfacial strength after enzymatic treatment in a cartilage transplantation model, Arthritis Res Ther 6(5) (2004) R469-76.
[24] S.N. Redman, G.P. Dowthwaite, B.M. Thomson, C.W. Archer, The cellular responses of articular cartilage to sharp and blunt trauma, Osteoarthritis Cartilage 12(2) (2004) 106-16.
[25] P.K. Bos, J. DeGroot, M. Budde, J.A. Verhaar, G.J. van Osch, Specific enzymatic treatment of bovine and human articular cartilage: implications for integrative cartilage repair, Arthritis Rheum 46(4) (2002) 976-85.
[26] A. Myngbay, Y. Bexeitov, A. Adilbayeva, Z. Assylbekov, B.P. Yevstratenko, R.M. Aitzhanova, B. Matkarimov, V.A. Adarichev, J. Kunz, CTHRC1: A New Candidate Biomarker for Improved Rheumatoid Arthritis Diagnosis, Front Immunol 10 (2019) 1353.
[27] V. Tillgren, J.C. Ho, P. Onnerfjord, S. Kalamajski, The novel small leucine-rich protein chondroadherin-like (CHADL) is expressed in cartilage and modulates chondrocyte differentiation, J Biol Chem 290(2) (2015) 918-25.
[28] S. Nuka, W. Zhou, S.P. Henry, C.M. Gendron, J.B. Schultz, T. Shinomura, J. Johnson, Y. Wang, D.R. Keene, R. Ramirez-Solis, R.R. Behringer, M.F. Young, M. Hook, Phenotypic characterization of epiphycan-deficient and epiphycan/biglycan double-deficient mice, Osteoarthritis Cartilage 18(1) (2010) 88-96.
[29] Y. Luo, D. Sinkeviciute, Y. He, M. Karsdal, Y. Henrotin, A. Mobasheri, P. Onnerfjord, A. Bay-Jensen, The minor collagens in articular cartilage, Protein Cell 8(8) (2017) 560-572.
[30] S. Bregant, C. Huillet, L. Devel, A.S. Dabert-Gay, F. Beau, R. Thai, B. Czarny, A. Yiotakis, V. Dive, Detection of matrix metalloproteinase active forms in complex proteomes: evaluation of affinity versus photoaffinity capture, J Proteome Res 8(5) (2009) 2484-94.
[31] R.H. Song, M.D. Tortorella, A.M. Malfait, J.T. Alston, Z. Yang, E.C. Arner, D.W. Griggs, Aggrecan degradation in human articular cartilage explants is mediated by both ADAMTS-4 and ADAMTS-5, Arthritis Rheum 56(2) (2007) 575-85.
[32] J.T. Sieker, B.L. Proffen, K.A. Waller, K.E. Chin, N.P. Karamchedu, M.R. Akelman, G.S. Perrone, A.M. Kiapour, J. Konrad, M.M. Murray, B.C. Fleming, Transcriptional profiling of articular cartilage in a porcine model of early post-traumatic osteoarthritis, J Orthop Res 36(1) (2018) 318-329.
[33] M.W. Lark, E.K. Bayne, J. Flanagan, C.F. Harper, L.A. Hoerrner, N.I. Hutchinson, Singer, II, S.A. Donatelli, J.R. Weidner, H.R. Williams, R.A. Mumford, L.S. Lohmander, Aggrecan degradation in human cartilage. Evidence for both matrix metalloproteinase and aggrecanase activity in normal, osteoarthritic, and rheumatoid joints, J Clin Invest 100(1) (1997) 93-106.
[34] F. Qu, J.M. Lin, J.L. Esterhai, M.B. Fisher, R.L. Mauck, Biomaterial-mediated delivery of degradative enzymes to improve meniscus integration and repair, Acta Biomater 9(5) (2013) 6393-402.
[35] J.S. Theodoropoulos, J.N. De Croos, S.S. Park, R. Pilliar, R.A. Kandel, Integration of tissue-engineered cartilage with host cartilage: an in vitro model, Clin Orthop Relat Res 469(10) (2011) 2785-95.
[36] E.A. Makris, D.J. Responte, N.K. Paschos, J.C. Hu, K.A. Athanasiou, Developing functional musculoskeletal tissues through hypoxia and lysyl oxidase-induced collagen cross-linking, Proc Natl Acad Sci U S A 111(45) (2014) E4832-41.
[37] A.A. Athens, E.A. Makris, J.C. Hu, Induced collagen cross-links enhance cartilage integration, PLoS One 8(4) (2013) e60719.
[38] F. Dell'accio, C. De Bari, N.M. Eltawil, P. Vanhummelen, C. Pitzalis, Identification of the molecular response of articular cartilage to injury, by microarray screening: Wnt-16 expression and signaling after injury and in osteoarthritis, Arthritis Rheum 58(5) (2008) 1410-21.

[39] S. Kalamajski, A. Oldberg, The role of small leucine-rich proteoglycans in collagen fibrillogenesis, Matrix Biol 29(4) (2010) 248-53.
[40] D. Chen, L.R. Smith, G. Khandekar, P. Patel, C.K. Yu, K. Zhang, C.S. Chen, L. Han, R.G. Wells, Distinct effects of different matrix proteoglycans on collagen fibrillogenesis and cell-mediated collagen reorganization, Sci Rep 10(1) (2020) 19065.
[41] J.M. Coles, L. Zhang, J.J. Blum, M.L. Warman, G.D. Jay, F. Guilak, S. Zauscher, Loss of cartilage structure, stiffness, and frictional properties in mice lacking PRG4, Arthritis Rheum 62(6) (2010) 1666-74.
[42] Q. Li, B. Han, C. Wang, W. Tong, Y. Wei, W.J. Tseng, L.H. Han, X.S. Liu, M. Enomoto-Iwamoto, R.L. Mauck, L. Qin, R.V. Iozzo, D.E. Birk, L. Han, Mediation of Cartilage Matrix Degeneration and Fibrillation by Decorin in Post-traumatic Osteoarthritis, Arthritis Rheumatol 72(8) (2020) 1266-1277.
[43] H.M. Ismail, J. Miotla-Zarebska, L. Troeberg, X. Tang, B. Stott, K. Yamamoto, H. Nagase, A.J. Fosang, T.L. Vincent, J. Saklatvala, Brief Report: JNK-2 Controls Aggrecan Degradation in Murine Articular Cartilage and the Development of Experimental Osteoarthritis, Arthritis Rheumatol 68(5) (2016) 1165-71.
[44] H.M. Deckx, S. Hatch, M. Robberechts, S. Dupont, J. Desrivot, H. Coleman, S. Larsson, A. Struglics, E.M. van der Aar, A. Fiew, FRI0539 A safety, tolerability, pharmacokinetics (PK) and pharmacodynamics (PD) study with increasing oral doses of glpg1972 administered daily for 29 days shows a strong biomarker effect in patients with KNEE and/or HIP OA, Annals of Rheumatic Diseases 77 (2018).
[45] A.S. Siebuhr, D. Werkmann, A.C. Bay-Jensen, C.S. Thudium, M.A. Karsdal, B. Serruys, C. Ladel, M. Michaelis, S. Lindemann, The Anti-ADAMTS-5 Nanobody((R)) M6495 Protects Cartilage Degradation Ex Vivo, Int J Mol Sci 21(17) (2020).
[46] F.G. Brunet, F.W. Fraser, M.J. Binder, A.D. Smith, C. Kintakas, C.M. Dancevic, A.C. Ward, D.R. McCulloch, The evolutionary conservation of the A Disintegrin-like and Metalloproteinase domain with Thrombospondin-1 motif metzincins across vertebrate species and their expression in teleost zebrafish, BMC Evol Biol 15 (2015) 22.
[47] A.J. McGregor, B.G. Amsden, S.D. Waldman, Chondrocyte repopulation of the zone of death induced by osteochondral harvest, Osteoarthritis Cartilage 19(2) (2011) 242-8.
[48] B. Sharma, S. Fermanian, M. Gibson, S. Unterman, D.A. Herzka, B. Cascio, J. Coburn, A.Y. Hui, N. Marcus, G.E. Gold, J.H. Elisseeff, Human cartilage repair with a photoreactive adhesive-hydrogel composite, Sci Transl Med 5(167) (2013) 167ra6.
[49] C. Salzlechner, T. Haghighi, I. Huebscher, A.R. Walther, S. Schell, A. Gardner, G. Undt, R.M.P. da Silva, C.A. Dreiss, K. Fan, E. Gentleman, Adhesive Hydrogels for Maxillofacial Tissue Regeneration Using Minimally Invasive Procedures, Adv Healthc Mater 9(4) (2020) e1901134.
[50] M.K. Boushell, C.T. Hung, E.B. Hunziker, E.J. Strauss, H.H. Lu, Current strategies for integrative cartilage repair, Connect Tissue Res 58(5) (2017) 393-406.
[51] P.H. Liebesny, K. Mroszczyk, H. Zlotnick, H.H. Hung, E. Frank, B. Kurz, G. Zanotto, D. Frisbie, A.J. Grodzinsky, Enzyme Pretreatment plus Locally Delivered HB-IGF-1 Stimulate Integrative Cartilage Repair In Vitro, Tissue Eng Part A 25(17-18) (2019) 1191-1201.
[52] Y. Perez-Riverol, A. Csordas, J. Bai, M. Bernal-Llinares, S. Hewapathirana, D.J. Kundu, A. Inuganti, J. Griss, G. Mayer, M. Eisenacher, E. Perez, J. Uszkoreit, J. Pfeuffer, T. Sachsenberg, S. Yilmaz, S. Tiwary, J. Cox, E. Audain, M. Walzer, A.F. Jarnuczak, T. Ternent, A. Brazma, J.A. Vizcaino, The PRIDE database and related tools and resources in 2019: improving support for quantification data, Nucleic Acids Res 47(D1) (2019) D442-D450.

Supplementary Methods

Explanation of n numbers for experimental assays

Explants from 2 pigs were used for metabolic labelling experiments. For experiments quantifying ADAMTS4 activity, data are biological replicates from 3 pigs/condition. For all other assays, explants from multiple pigs were pooled and randomly assigned to experimental conditions, as follows. Immunostaining for ADAMTS4 and Type II collagen, and Safranin-O/Sirius Red staining were performed on Core/Disc explants taken from a pool created from 10 pigs. SEM imaging (no freeze/thaw) or TIMP-3 treatment was performed on explants taken from 5 pigs. Assessment of integration by Safranin-O staining in Sheathed Cut explants, and Safranin-O staining, SEM and metabolic labelling in devitalized explants (with or without enzyme treatment), were performed on explants pooled from 4 pigs. Live/dead staining, tensile failure tests (control vs. TIMP-3 inhibition), pSILAC proteomics and safranin-O staining on control and TIMP-3-inhibited explants were performed using explants pooled from 6 pigs. Tensile failure tests on freeze/thaw and/or enzymatic treatment explants were pooled from 12 pigs. Gene expression analyses were performed on explants pooled from 9 pigs. In total, 51 pigs were used.

Protein extraction and MS sample preparation

Explants were dissected using two parallel blades glued to either side of a microscope slide. Injured samples were aligned so that the integration area was equidistant between the two parallel blades to isolate the integration tissue. After dissection, tissue was snap frozen in liquid nitrogen and stored at -80 °C. Cartilage explants were placed in homogenization tubes containing 0.4M Tris buffer (pH 8) containing phosphatase inhibitors (PhosSTOP, Sigma) and

protease inhibitor cocktail (cOmplete Mini, EDTA-free, Roche). Explants were then homogenized on a Precellys Evolution/Cryolys, cycling 7 times for 20s at 6800 rpm followed by a 30s pause at 0 °C. 5µL of 100mM dithiothreitol (DTT) was then added and the resulting solution heated to 65 °C for 15min before being allowed to cool to RT. 20µL 200mM of Iodoacetamide (Sigma) was then added and incubated at RT for 30min before 50µL of DTT was added to quench at RT for 30min. The resulting pellet was then resuspended in 50µL of 4M GuHCL buffer (in 0.1M Tris buffer, pH 5.8) on an IKA mixer (2000rpm) for 2h at RT. Proteins were then digested in Trypsin (Promega, 1:50 ratio trypsin:protein (w/w)) overnight at 37 °C. Digestion was terminated by acidifying the solution with trifluoroacetic acid to a final concentration of 0.5% and particulates were removed by centrifugation at 4 °C at 14,000-16,000g for 10min. Peptides were then purified on SOLA C18 solid phase extraction cartridges (Thermo Fisher Scientific) and dried in a SpeedVac. Peptides were then dissolved in 20µL loading buffer before being loaded for mass spectrometry analysis.

Liquid Chromatography-Tandem Mass Spectrometry (LC-MS/MS)

Samples were analyzed on a LC-MS/MS platform consisting of Orbitrap Fusion Lumos coupled to an UPLC ultimate 3000 RSLCnano (Thermo Fisher Scientific). Samples were loaded in 1% acetonitrile and 0.1% (v/v) trifluoroacetic acid and eluted with a gradient from 2 to 35% acetonitrile in 0.1% (v/v) formic acid and 5% (v/v) DMSO in 60min with a flow rate of 250nL/min on a 50cm EASY-Spray column (ES803, Thermo Fisher Scientific).

The survey scan was acquired at a resolution of 120,000 between 400-1500m/z and an AGC target of 4E5. Selected precursor ions were isolated in the quadrupole with a mass isolation window of 1.6 Th and analyzed after CID fragmentation at 35% normalized collision energy in the linear ion trap in rapid scan mode. The duty cycle was fixed at 3s with a maximum

injection time of 35ms with AGC target of 4000 and parallelization enabled. Selected precursor masses were excluded for the following 27s.

MaxQuant software[1] (V1.6.7.0) was used to search the raw mass spectral data files. SILAC (Lys8Arg10) was set for quantitation. Fixed modification was carbamidomethylation of cysteine; and variable modifications were oxidized methionine, deamidation of asparagine and glutamine, and hydroxylation of proline. The data was searched against the porcine canonical Uniprot database (14/03/2021). A false discovery rate (FDR) on peptide and protein level were set to 1%. All other parameters were left at default settings. Perseus v1.6.14.0 was used to perform data analyses and statistical testing using the MaxQuant proteingroups.txt file as input. Only proteins with valid H/L ratio values in all replicates were used for analyses. H/L ratios were log2 transformed then normalized within each replicate by median subtraction. p-values and q-values were produced using a two-sided Student's t-test and a permutation-based FDR (0.05, 250 randomizations).

1. Tyanova, S., Temu, T. & Cox, J. The maxquant computational platform for mass spectrometry-based shotgun proteomics. Nat Protoc, 2016;11:2301-19.

Supplementary Figures and Tables

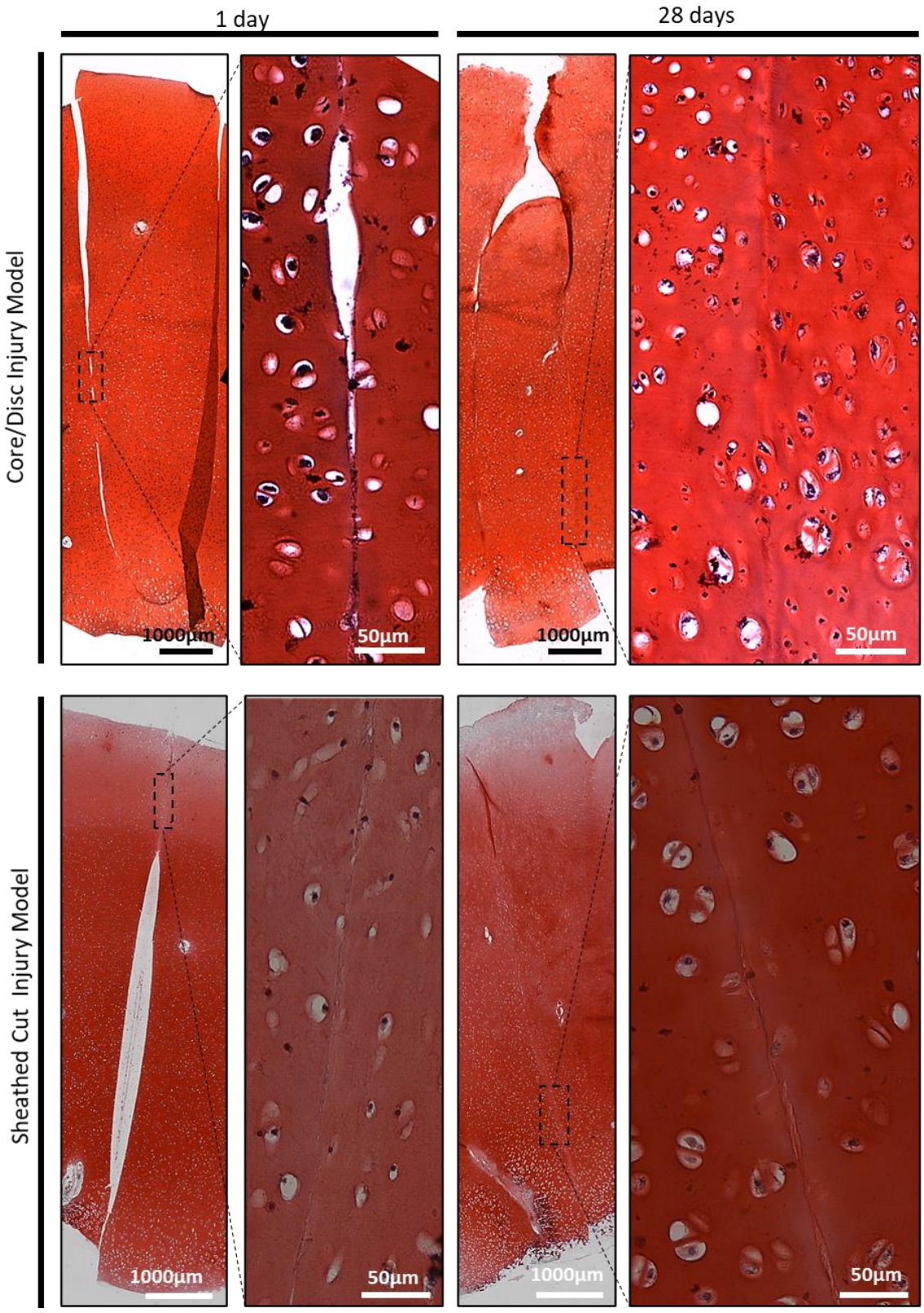

Supplementary Fig. 1. Representative cartilage explant sections stained with Safranin-O and haematoxylin showing integration in both the Core/Disc and Sheathed Cut injury models. The Core/Disc model has been previously described by van Osch (Janssen et al. 2006), but the core can slip within the disc, resulting in areas that integrate poorly. Our improved 'Sheathed Cut' model avoids this issue, leading to more consistent integration. In both models, some integration is visible at day 1, but by day 28, many areas appear to be well integrated. Some panels also appear in Fig. 1c and are reproduced here for comparison.

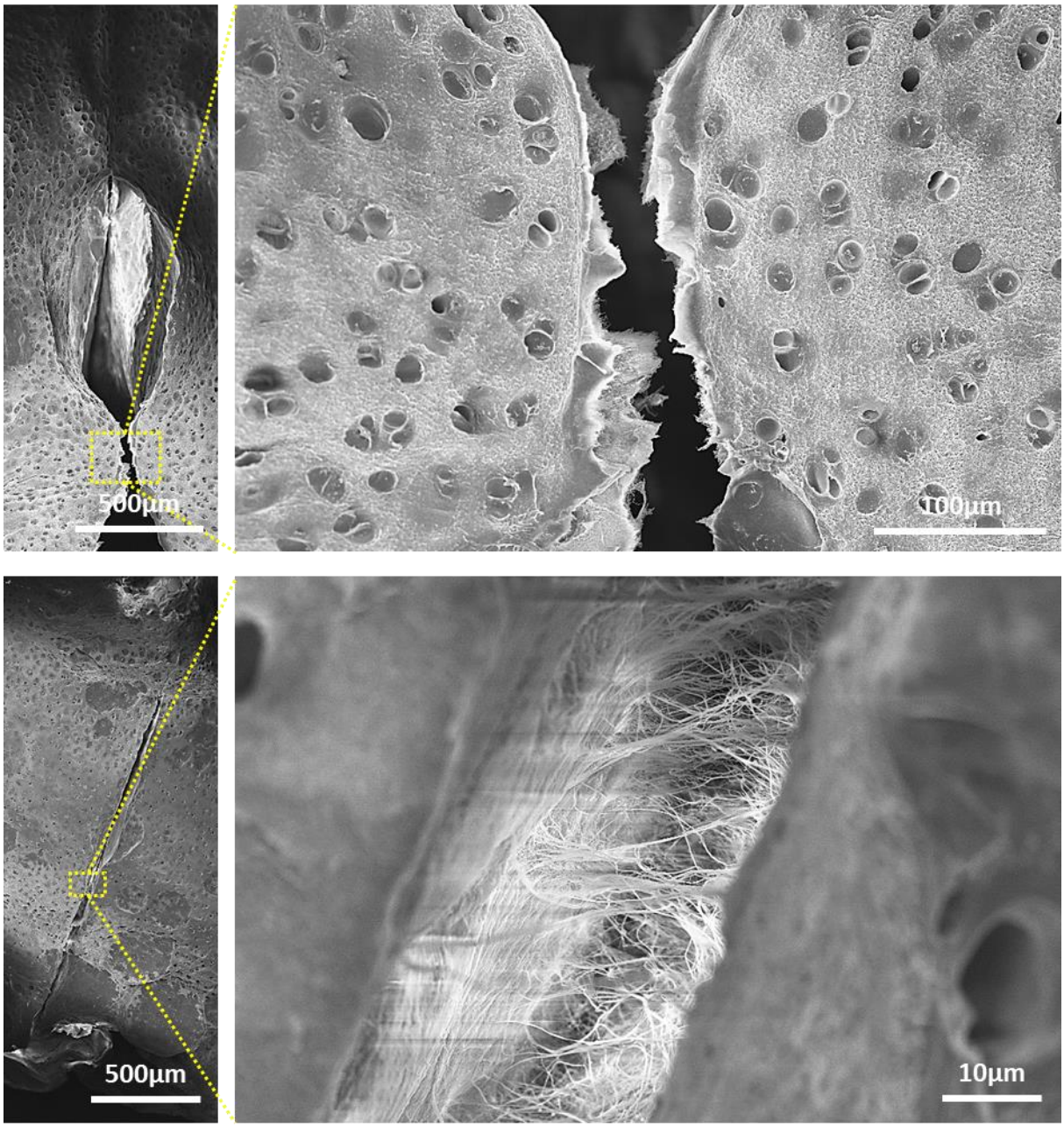

Supplementary Fig. 2: Additional representative SEM images of the integration surface in a Sheathed Cut explant after 28 days in culture. Total integration along the full length of the cut surfaces was rarely observed. Moreover, freezing samples for cryosectioning often resulted in what appeared to be fracturing (top) or pulling apart (bottom) of areas that appeared to have been previously integrated.

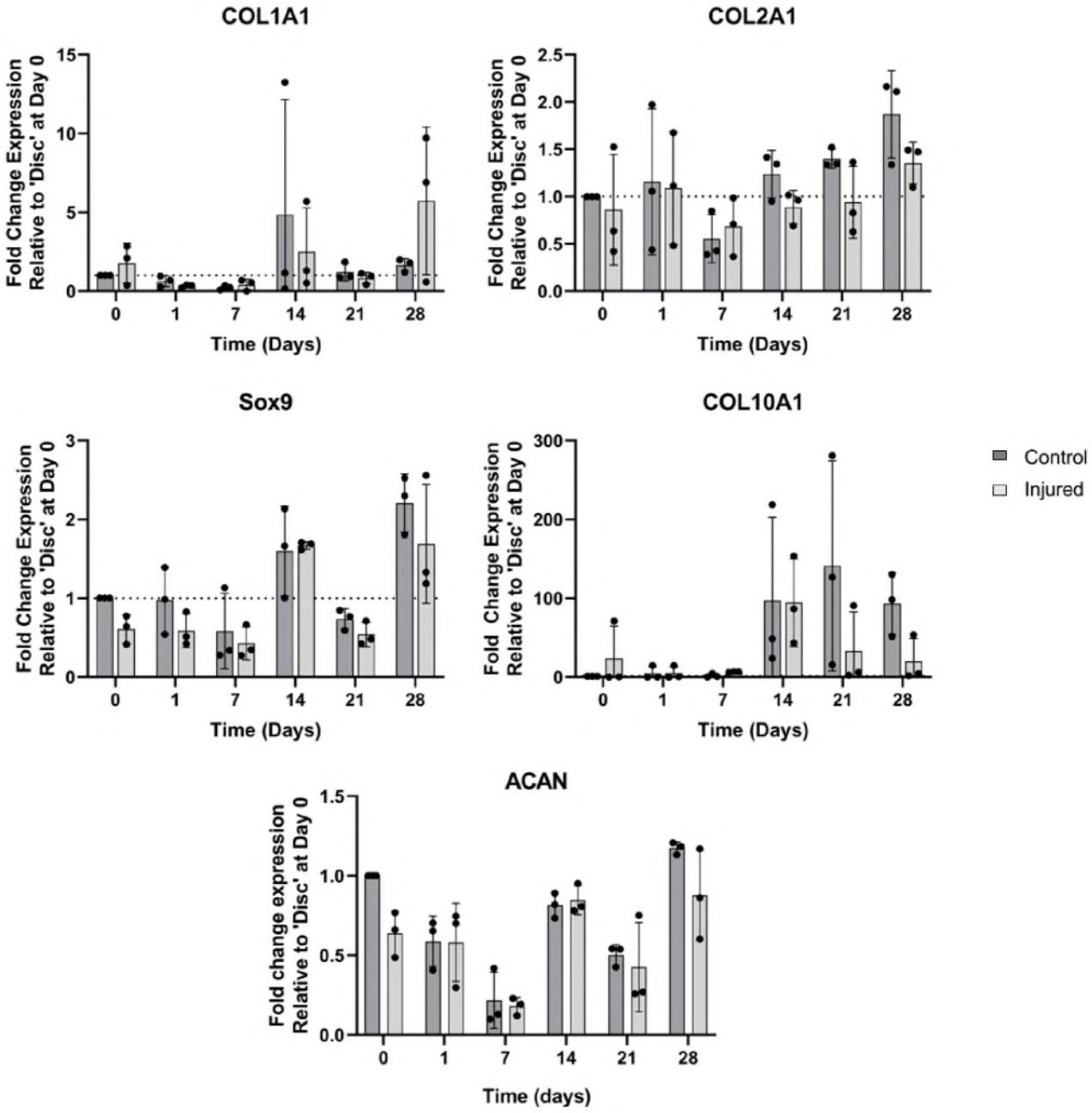

Supplementary Fig. 3: qPCR for genes encoding types I, II, or X collagen, aggrecan, and the transcription factor Sox9 in Control (uninjured Disc) and corresponding Injured (Core/Disc) explants. Control was no different from Injured for any gene at any time point (n=3, unpaired two-tailed t-test, $p>0.05$). Bars show means ± SD.

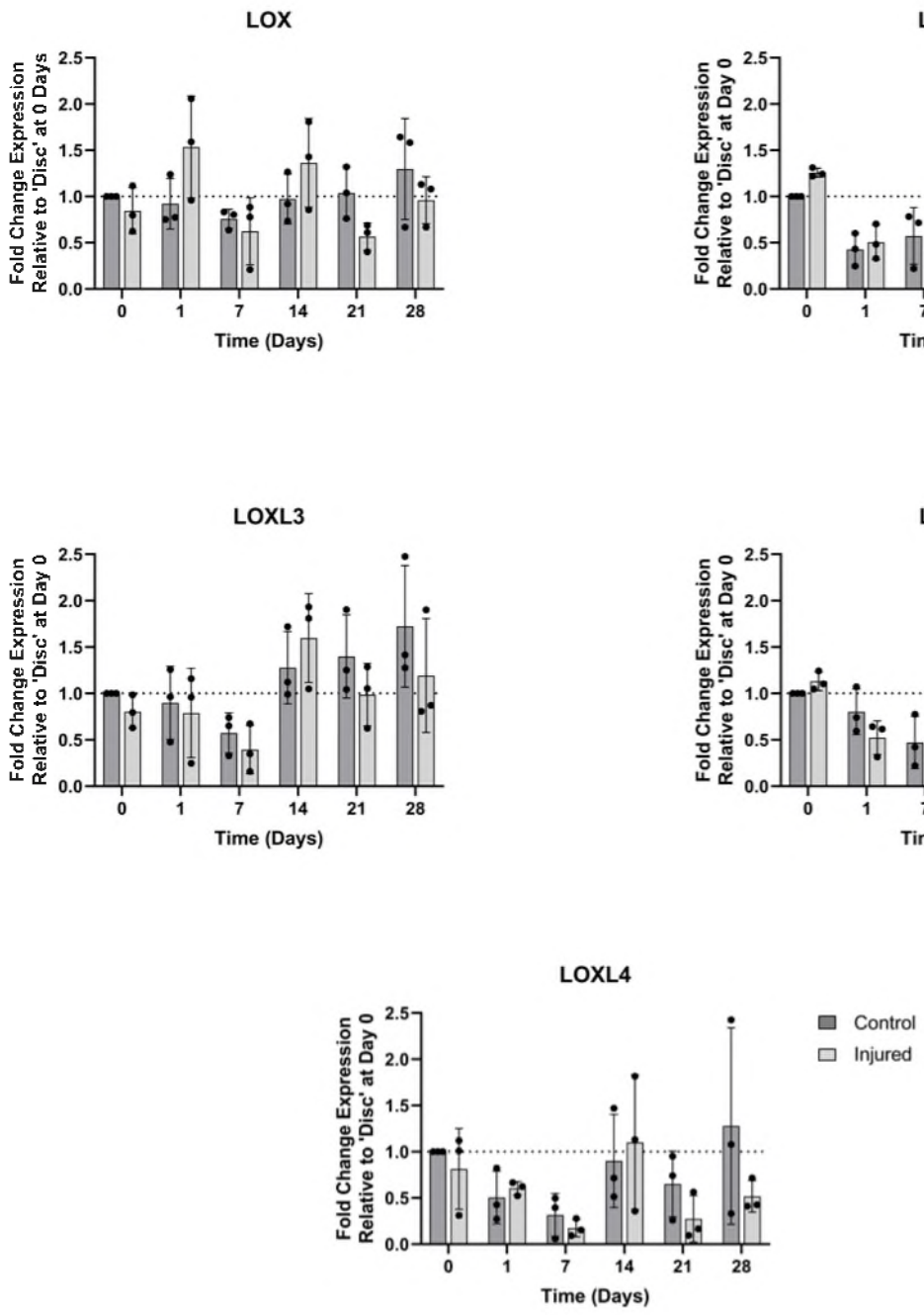

Supplementary Fig. 4: qPCR for genes encoding LOX enzyme and its isoforms in Control (uninjured Disc) and corresponding Injured (Core/Disc) explants. Control was no different from Injured for any gene at any time point (n=3, unpaired two-tailed t-test, $p>0.05$). Bars show means ± SD.

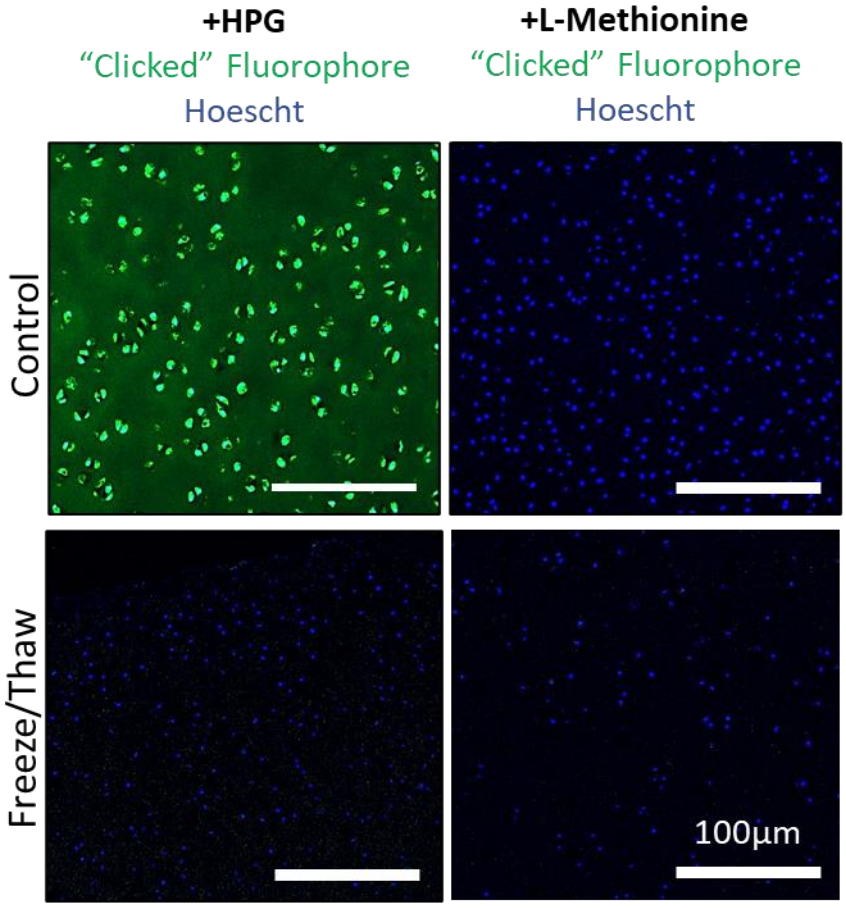

Supplementary Fig. 5: Representative fluorescence images of cartilage explant tissue sections in which a non-canonical amino acid tagging technique was performed to visualize newly synthesized proteins. Cartilage explants were either cultured as normal (Control) or devitalized by a freeze/thaw cycle. Explants were placed in culture media supplemented with either HPG or L-methionine and cultured for 48h. A "click" reaction was then performed on sections to attach a fluorophore to non-canonical amino acid (HPG) that had been incorporated into neo-proteins and sections imaged using confocal microscopy.

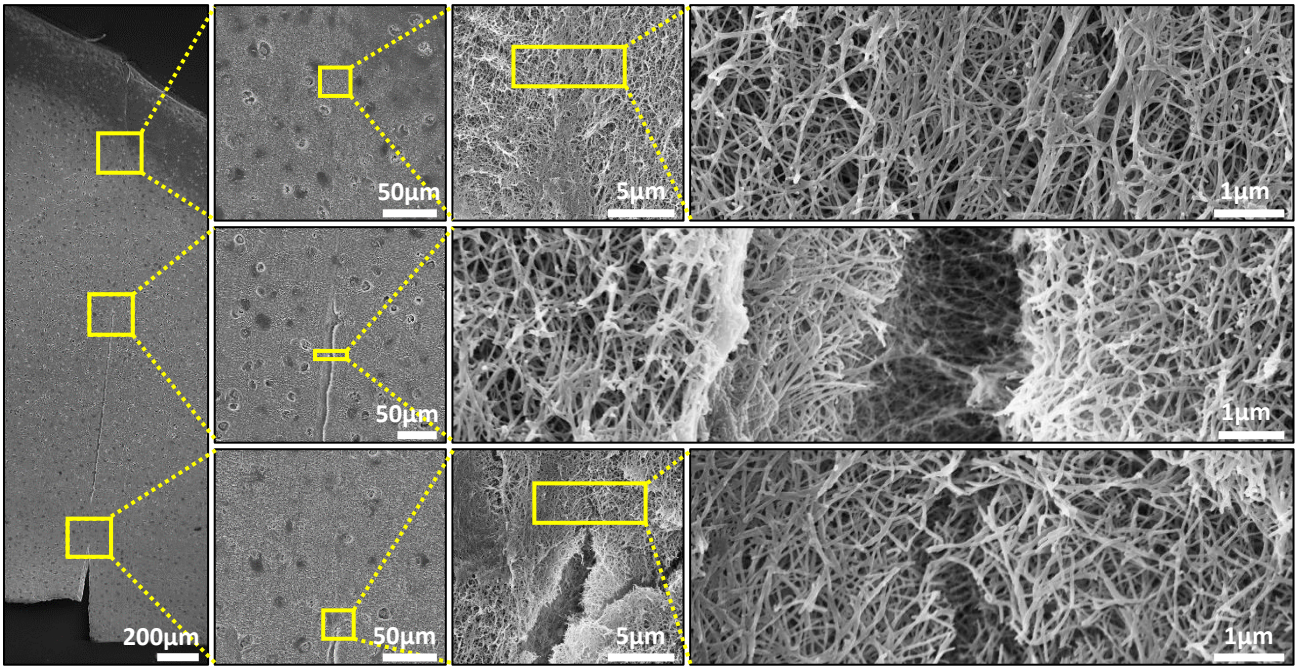

Supplementary Fig. 6: Representative scanning electron microscopy images across the defect of a Sheathed Cut explant after 1 freeze/thaw cycle and enzymatic treatment after 23 days of culture in deionized water. Integrated areas show fibrils spanning the defect (n=4 explants, from pool collected from 4 pigs).

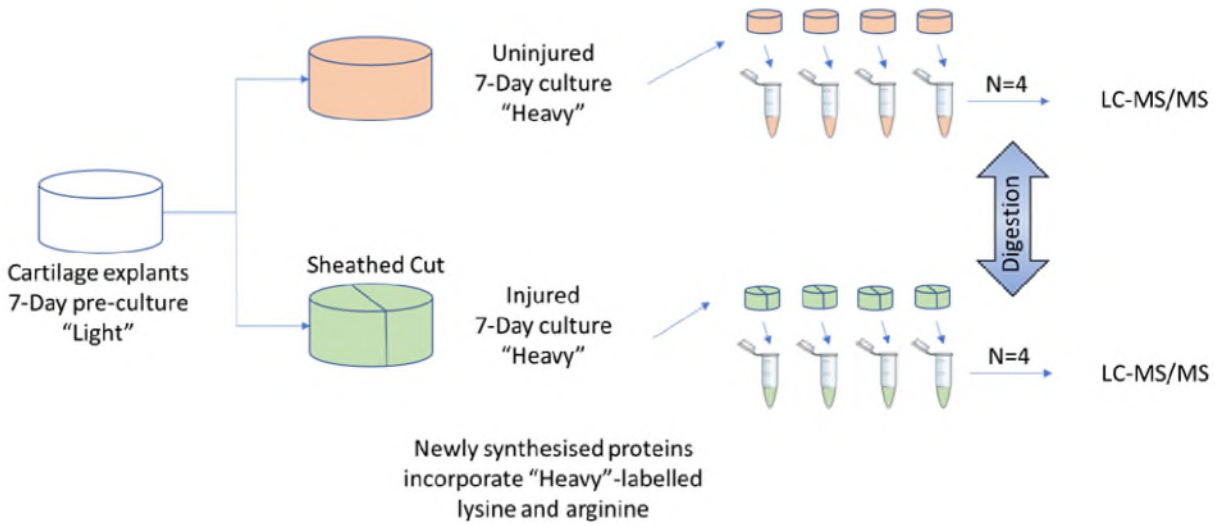

Supplementary Fig. 7: Experimental setup describing how pulsed SILAC was performed on Sheathed Cut explants to identify newly synthesized proteins.

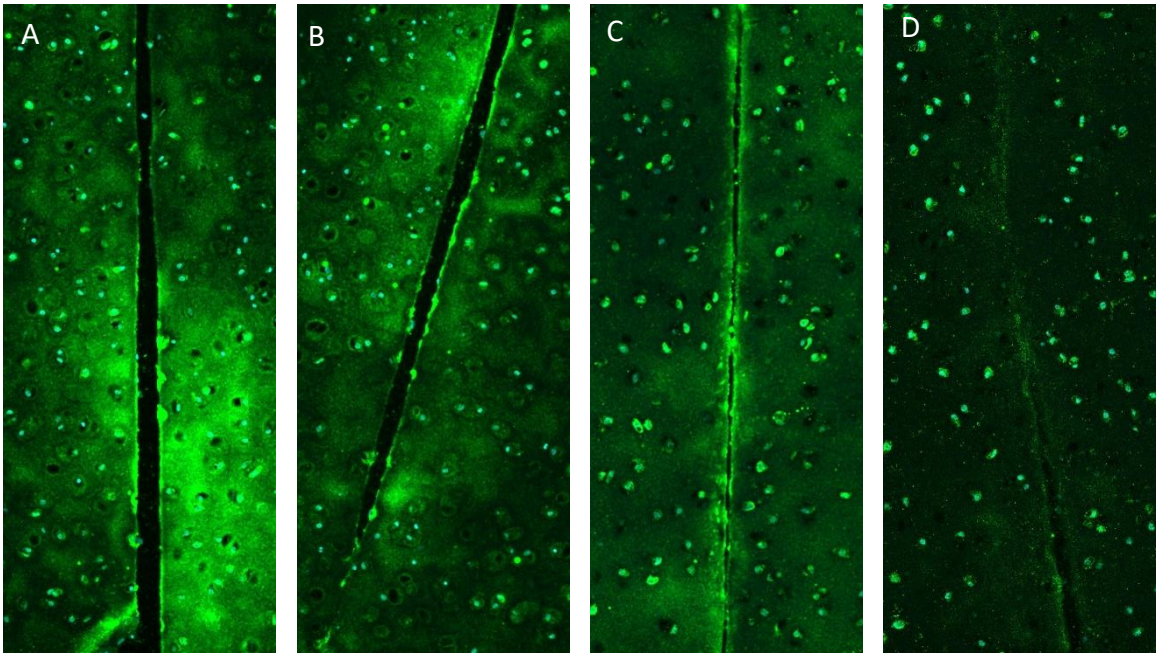

Supplementary Fig. 8: Additional representative confocal images showing immunostaining for ADAMTS4 along the cut surfaces of a Core/Disc explant 24h after injury. ADAMTS4 was found at the injury interface in all samples 24h after injury (**A-C**), however minimal staining was observed after 28 days of culture (**D**). n=3 explants, from pool collected from 10 pigs

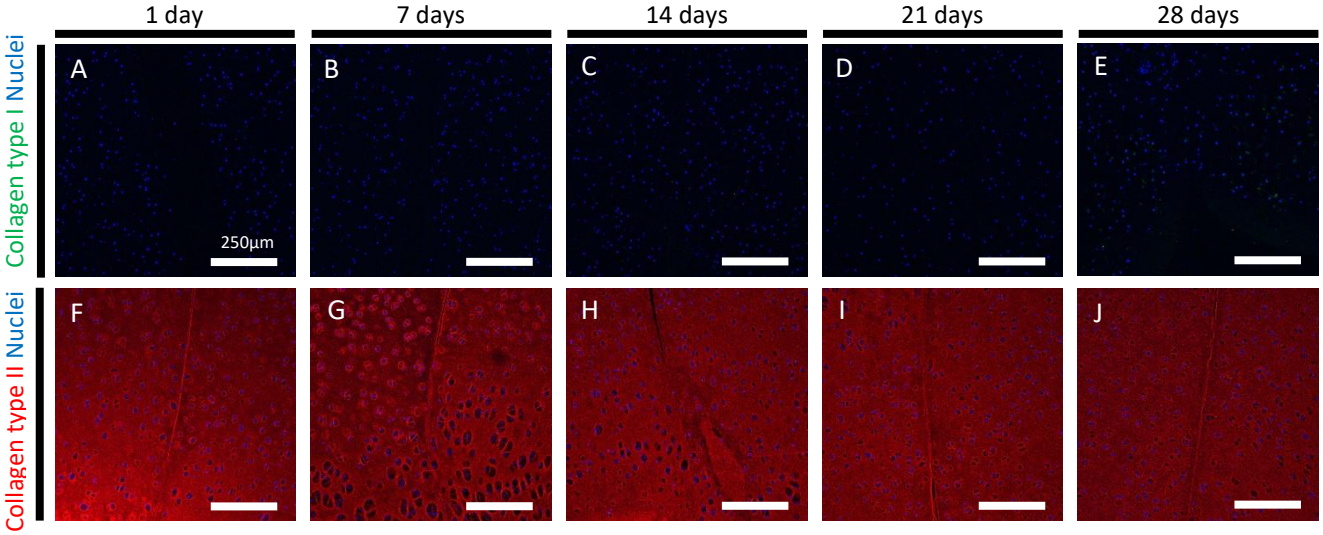

Supplementary Fig. 9: Representative confocal images along cut surface showing immunostaining for types I and II collagen in a Core/Disc model after 28 days in culture. (n=3 explants, from pool collected from 10 pigs).

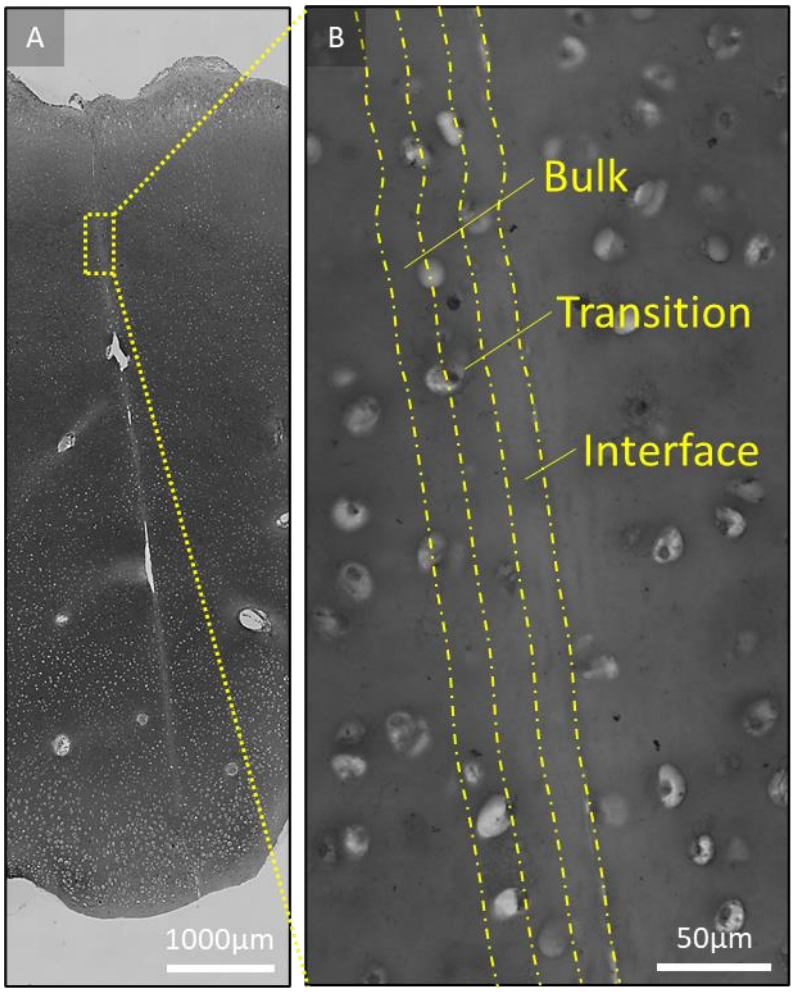

Supplementary Fig. 10: Diagram overlaid on section from a Sheathed Cut explant demonstrating how Safranin-O staining intensity quantification was carried out in regions 50µm from cut surface. The interface area was taken as the first 50µm from the cut surfaces, the transition zone was the next 50µm, and bulk an additional 50µm.

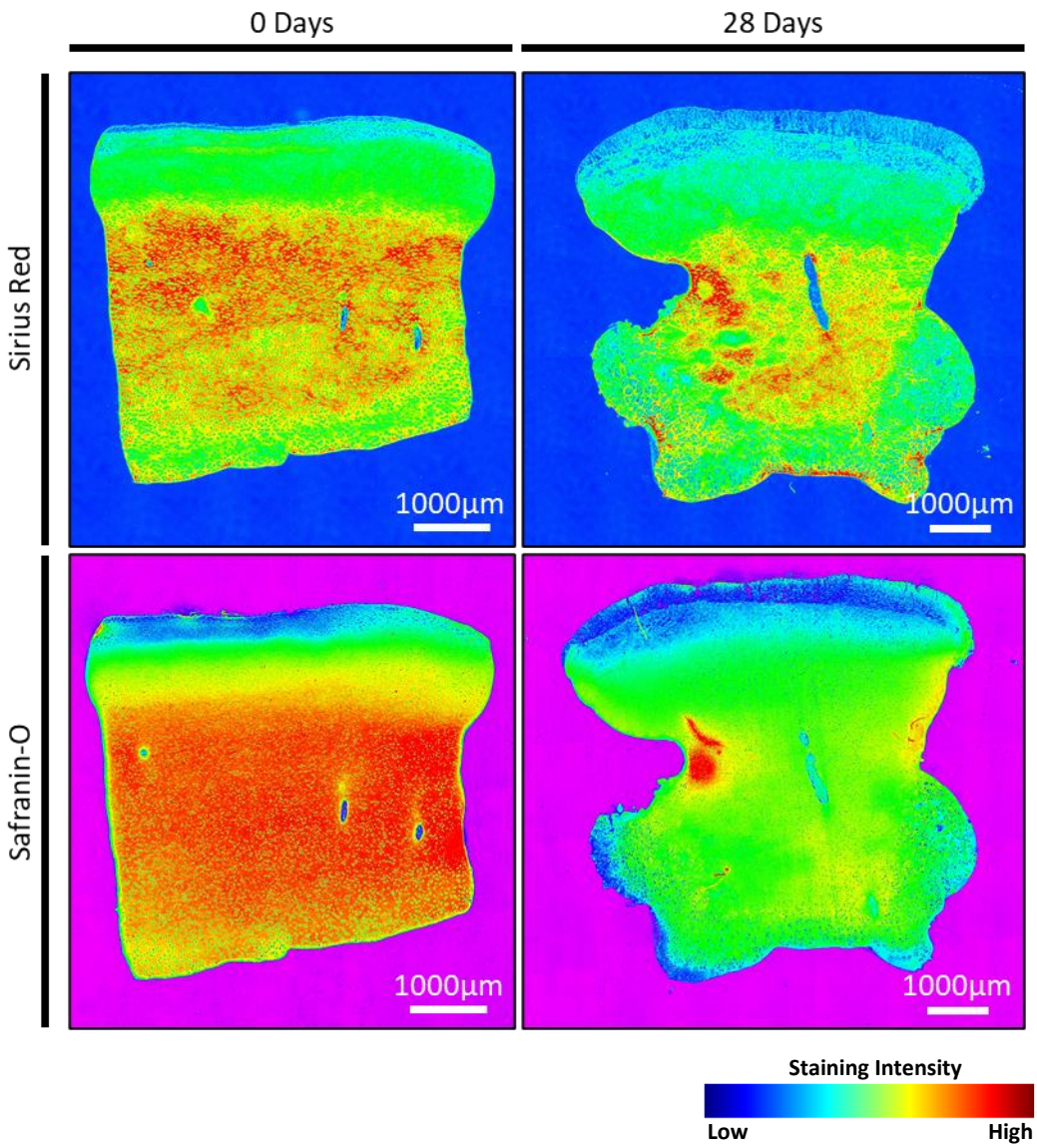

Supplementary Fig. 11: Representative sections of uninjured cartilage explants after 0 and 28 days in culture stained for Sirius Red (collagens) and Safranin-O (proteoglycans) and false colored according to staining intensity. In line with joint immobilization studies (*e.g.*, Nomura *et al*. *Osteoarthritis Cartilage,* 2017), proteoglycans are quickly lost while the collagen network remains relatively intact.

Proteoglycans Collagen

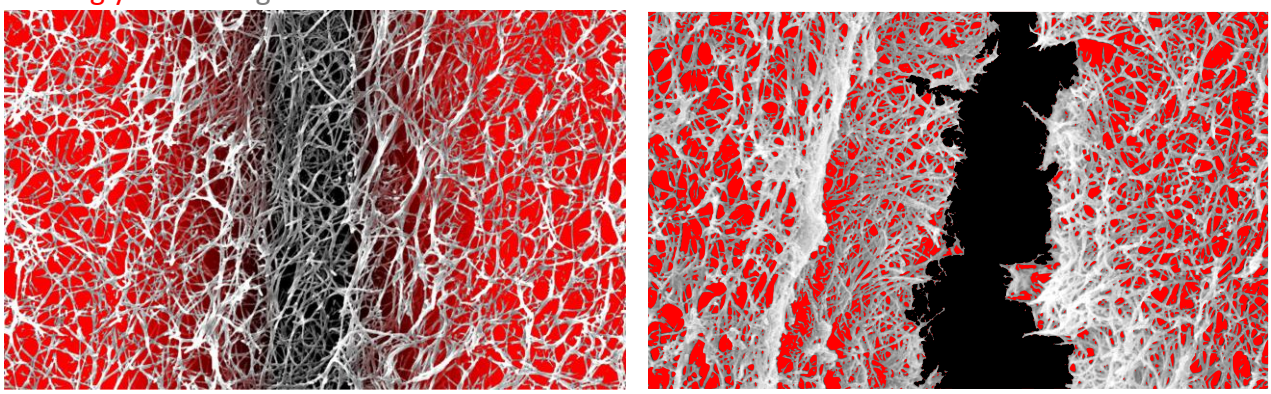

Supplementary Fig. 12: Schematic highlighting proposed mechanism of cartilage repair. (left) Integration was evident when proteoglycan were depleted near the injury interface either through treatment with exogenous enzymes (in freeze/thawed samples) or in living samples where aggrecanases were not inhibited. (right) Collagen integration was not observed when proteoglycans remained in the interface zone.

Supplementary Table 1: Primers used for gene expression analyses.

GENE	FORWARD	REVERSE	NCBI ACCESSION NUMBER
ACAN	TATGAGGACGGCTTCCACCA	CTTGTCCCCGTAGCAACCTT	NM_00116 4652.1
BGN	GGCCGGTAGGTGGAGGTAAT	GGACATGACAAGTGGGCTGG	XM_01398 6528.2
COL1A1	CAACCGCTTCACCTACAGC	TTTTGTATTCGATCACTGTCTTGCC	
COL2A1	GCGGCTTCCATTTCAGCTATG	GCTTTCTTGAGGTTGCCAGC	XM_02109 2611.1
DCN	GCTCAGGCATTGAAAACGGA	GGAAGACCTTGAGGGATGGT	NM_21392 0.1
EPYC	AATTCACTGGGGTTCTGGGC	ATGGTCGTCACAGTACACGG	XM_02109 3029.1
FMOD	TCACGATGATGTGGTGCCAT	AAGCGCTGCTCACATAGTCA	XM_00313 0105.4
KERA	ATGGCGACCCCAATCTGTTT	AACCTGCCTCACACTTCGAG	XM_00192 7128.5
LOX	AAGGTCAGTGTGAACCCCAG	GCGAATTTCACAGCGAACGA	NM_00120 6403.1
LOXL1	GTGCAGCCTGGGAACTACAT	GTTGCAGAAACGTAGCGACC	XM_00566 6170.3
LOXL2	GGAGAAGACGTACAACGCCA	TGTGCAGTCCATGGAGAACG	XM_02107 4114.1
LOXL3	TATGACGGCCATCGCATCTG	CTGGCCAGGATAGCGTTCAA	XM_02108 7325.1
LOXL4	CAGCGATGCTCCTGTCATCA	CTCATCAGCCTGGATTTGGGG	XM_02107 4442.1
LUM	TCCGTCCTGACAGAGTTTACAG	GTCGCCAAGAGGAGAGTAAACA	NM_00124 3339.1
RPL13A	GGCCTTGTTTACTGCTGGTC	GGTTCACTCCTGCCAACAAC	NM_00124 4068.1
SOX9	GAAGGACCACCCGGATTACAA	GAAGATGGCGTTGGGAGAGAT	NM_21384 3.2
ADAMTS4	GGGGGATCTCTGTTAGGGGT	AGAGTTAGGGGTGCCTCCTT	NM_00116 4652.1

Protein names	Gene names	log2 ratio H/L Control_01	log2 ratio H/L Control_02	log2 ratio H/L Control_03	log2 ratio H/L Control_04	log2 ratio H/L Injury_01	log2 ratio H/L Injury_02	log2 ratio H/L Injury_03	log2 ratio H/L Injury_04	Razor + unique peptides	Unique + razor sequence coverage [%]	Mol. weight [kDa]	Andromeda search engine score	-log10 p value	p value	-log10 q value	q value	Student's T-test Difference log2 fold change Injury / Control	Intensity	Intensity L	Intensity H	iBAQ L Control1	iBAQ H Control 1
[illegible]	ACAN	-1.8045	-2.0268	-1.5941	-2.0443	-2.3004	-1.8088	-1.9798	-1.6398	#	25	237.6	323.3	0.139	0.7261	0.0808	0.8303	-0.0648	10.0305	9.98932	8.98662	7.25074	6.37449
[illegible]	ACLY	0.05508	0.41917	0.78744	0.68402	-0.0218	0.61122	1.40042	-0.3006	#	17	123.7	181	0.0549	0.8813	0.0169	0.9618	-0.0641	7.52599	7.33788	7.07196	5.06345	4.74099
[illegible]	ACTA2	0.3667	0.06715	0.42568	-0.1226	-0.3346	-0.087	-0.2291	-0.3604	#	50	41.46	88.42	1.6497	0.0224	0.7615	0.1732	-0.437	9.13098	8.99444	8.56192	6.84346	6.54872
[illegible]	ACTG1	-0.2636	0.09297	0.03924	-0.28	0.12373	-0.0496	-0.203	-0.1025	5	24	40.1	279	0.1428	0.7198	0.0772	0.8371	0.045	8.73329	8.61474	8.11143	6.15936	5.74149
[illegible]	ACTN4	1.22582	0.75303	0.81139	0.75503	0.92271	0.72453	0.98389	0.91186	#	27	107.3	116.8	0.0015	0.9966	0.0019	0.9957	-0.0006	7.99844	7.80275	7.55806	5.05668	4.866
[illegible]	AHNAK	1.02735	1.39106	1.57453	1.40089	2.01195	1.82107	1.73499	0.54975	7	12	235.8	9.968	0.2044	0.6246	0.1105	0.7753	0.18098	7.66377	7.36152	7.36395	3.49041	3.35985
[illegible]	ALDOA	1.72799	1.05087	0.85438	1.42208	0.65236	0.99689	0.75823	0.94159	#	33	39.82	238.6	1.0517	0.0888	0.5555	0.2783	-0.4266	8.01153	7.786	7.61907	5.4414	5.483
[illegible]	ALDOC	0.92311	1.26579	0.9677	1.11364	0.72156	0.64593	1.16966	0.93962	5	17	46.85	74.51	0.6787	0.2096	0.4078	0.391	-0.1984	7.4178	7.20602	7.00432	4.91148	4.77905
[illegible]	ANGPTL2	1.16246	1.71509	2.29684	2.12913	1.17307	1.8	0.78256	0.93377	9	22	56.95	148.6	0.995	0.1012	0.5427	0.2866	-0.6535	7.63773	7.33201	7.34134	5.12222	5.09146
Annexin	ANXA11	0.58689	-0.0042	-0.0695	0.19178	0.29819	0.6024	1.31716	0.38406	4	10	53.94	6.236	0.8706	0.1347	0.5105	0.3087	0.4742	7.21767	7.08153	6.64759	4.58966	4.19915
Annexin	ANXA2	-0.1782	-0.2725	-0.5974	-0.6989	-0.5146	-0.2229	-0.2132	-0.5307	#	51	38.58	91.01	0.1677	0.6796	0.0886	0.8154	0.06641	8.64332	8.54468	7.95124	6.18704	5.71787
[illegible]	ANXA4	-0.5257	-0.8431	-1.3027	-1.583	-0.5542	1.15705	0.40837	-1.0323	7	26	35.83	9.774	1.0027	0.0994	0.5433	0.2862	1.05835	7.88182	7.6839	7.44532	5.0149	4.37543
Annexin	ANXA5	-0.2364	-0.5528	-0.5018	-0.7477	-0.8117	-0.3106	-0.9657	-0.6671	#	60	36.13	169.5	0.4607	0.3462	0.2631	0.5456	-0.1791	8.83834	8.74729	8.11511	6.49574	5.98099
Annexin	ANXA6	-0.93	-1.1836	-1.2329	-0.6484	-0.5172	-0.8137	-0.2356	0.11717	#	38	72.12	48.12	1.4219	0.0379	0.7105	0.1948	0.63637	7.93728	7.85857	7.15679	5.23709	4.64485
Annexin	ANXA8	1.76728	2.01933	1.44796	2.54043	1.16813	2.00202	0.98481	1.10914	#	49	36.75	97.62	0.9856	0.1034	0.55	0.2819	-0.6277	8.1051	7.81433	7.79355	5.6638	5.72865
[illegible]	APOD	0.79459	0.49698	0.83907	0.86013	2.39059	1.91039	1.87793	0.93355	4	35	20.37	44.59	1.761	0.0173	0.8329	0.1469	1.03042	7.793	7.54449	7.4322	5.66079	5.50151
[illegible]	ARHGDIA	-0.0309	-0.2349	-0.1681	-0.2162	-0.8081	0.55046	0.59041	-1.1593	4	22	30.2	75.78	0.0333	0.9262	0.0064	0.9854	-0.0441	7.86195	7.74865	7.22298	5.31969	4.96855
[illegible]	ATP5F1A	0.6174	0.91247	1.28129	0.72687	0.927	0.39313	0.28308	0.61297	6	14	58.25	17.76	0.8088	0.1553	0.492	0.3221	-0.3305	7.77937	7.58929	7.32891	5.31431	5.0472
[illegible]	ATP5F1B	0.47203	0.87728	1.18238	0.83834	0.98128	0.51797	0.28674	0.4181	9	28	48.64	10.51	0.6697	0.2139	0.4068	0.3919	-0.2915	7.40564	7.19393	6.99205	4.64277	4.42778
Biglycan	BGN	-1.9335	-2.1071	-2.1125	-2.1793	-2.2629	-2.0842	-2.0439	-2.1151	#	52	37.63	323.3	0.2493	0.5632	0.1395	0.7252	-0.0434	10.0522	10.0222	8.87643	7.79562	6.72104
Basigin	BSG	1.4899	2.20284	1.71403	1.96797	1.33625	1.73642	1.63336	1.26854	3	13	27.22	6.703	0.9303	0.1174	0.5392	0.2889	-0.35	7.36314	7.05846	7.06569	5.10243	5.10992
[illegible]	C1QC	-1.5299	-1.6702	-1.8491	-0.6336	-1.262	-0.5407	-2.6252	0.01712	6	36	26.02	155.2	0.1988	0.6327	0.1125	0.7718	0.31798	8.24873	8.22383	6.99489	5.92734	4.87248
[illegible]	CALR	0.29575	0.2041	0.35301	0.73207	0.11821	0.81194	0.24045	0.28298	7	27	42.61	79.34	0.0604	0.8701	0.0185	0.9583	-0.0328	8.09513	7.93631	7.58128	6.01022	5.67541
[illegible]	CALU	0.72523	0.81745	0.69716	0.81542	0.68605	0.55342	0.74412	0.83317	#	37	44.42	82.83	0.3945	0.4032	0.2304	0.5883	-0.0596	8.36339	8.17094	7.91723	5.87999	5.58448
Calnexin	CANX	0.42761	1.01543	1.14673	0.87058	0.78548	0.74129	1.03018	0.46088	6	13	63.17	10.22	0.2282	0.5912	0.1312	0.7393	-0.1106	7.75198	7.60342	7.21394	5.42333	4.91131
[illegible]	CCDC80	0.15055	0.04538	0.01294	0.53057	-0.4107	0.59774	0.84064	-0.3844	#	18	108.5	24.02	0.0236	0.9471	0.0043	0.99	-0.024	7.95474	7.83535	7.3356	5.26919	4.87263
[illegible]	CFL1	0.71552	0.70286	0.21428	0.78051	0.94873	0.5492	0.96561	0.37286	5	39	18.52	32.31	0.2139	0.611	0.1205	0.7577	0.10581	7.77441	7.59089	7.31178	5.74681	5.42854
[illegible]	CHAD	-0.9251	-1.6934	-0.8675	-1.4184	-1.8137	-1.8511	-1.7073	-1.3663	#	49	40.62	323.3	1.0438	0.0904	0.5586	0.2763	-0.4585	9.24272	9.18682	8.3248	7.14836	6.47631
[illegible]	CHADL	-1.4997	-1.4162	-1.7736	-1.8655	-1.208	-1.4714	-1.0604	-1.1152	#	23	81.12	50.64	1.6293	0.0235	0.8114	0.1544	0.425	8.46731	8.42513	7.43374	5.89341	4.96774
[illegible]	CHI3L1	0.93883	1.02718	0.50115	0.99103	1.61886	0.50634	2.05377	1.68926	#	27	47.13	39.07	0.8496	0.1414	0.4967	0.3186	0.60251	8.71974	8.51929	8.28758	5.43189	5.26752
[illegible]	CILP2	0.60669	0.00633	-0.2127	-0.4909	0.66643	-0.9823	1.22984	-0.6601	#	29	127.1	323.3	0.0524	0.8863	0.0167	0.9622	0.08609	8.48854	8.25154	8.1124	5.03527	4.83707
[illegible]	CKAP4	-0.1825	-0.1515	-0.3805	-0.261	-0.6456	-0.2605	-0.6051	-0.0243	#	55	64.54	323.3	0.3927	0.4049	0.2316	0.5867	-0.14	9.2686	9.06172	8.84718	6.62851	6.49084
[illegible]	CLEC3A	-0.9039	-0.6298	-0.987	-0.401	-1.4279	-1.6203	-0.7435	-1.1883	8	45	21.98	259.1	1.1674	0.068	0.643	0.2275	-0.5146	8.9314	8.8635	8.09198	6.95672	6.21867
[illegible]	CLTC	0.92664	0.55026	0.48493	0.20904	2.63588	0.51234	0.3348	1.17041	#	14	188.6	117.8	0.5276	0.2968	0.3185	0.4803	0.62064	7.75841	7.54902	7.3411	4.78798	4.64744
[illegible]	CNMD	-2.5399	-2.6323	-2.487	-2.9131	-3.2665	-2.5208	-2.3193	-3.0183	3	18	37.29	78.01	0.2342	0.5832	0.1267	0.747	-0.1381	9.20118	9.1813	7.85217	6.94812	5.74872
[illegible]	CNPY2	-0.1542	-0.4823	-0.0128	-0.1269	-0.9724	-0.6549	-0.0823	0.97385	5	39	20.67	5.928	0.0077	0.9823	0	1	0.01014	7.50622	7.4063	6.81911	5.42267	4.87013
[illegible]	COL11A1	-1.3333	-0.8279	-2.1825	-1.8696	-2.4409	-1.5022	-2.3723	-2.7322	#	29	182.1	323.3	0.8985	0.1263	0.515	0.3055	-0.7086	10.3802	10.3319	9.40248	7.4983	6.79311
[illegible]	COL11A2	-1.3982	-1.6398	-1.9553	-2.218	-2.394	-1.1584	-2.5339	-2.7645	#	39	178.2	323.3	0.4596	0.3471	0.2667	0.5411	-0.4099	10.5407	10.5034	9.45558	7.62937	6.76115
[illegible]	COL12A1	0.7002	0.60268	0.83334	0.07987	-0.4799	1.48523	-0.6111	-0.1639	#	42	332.8	323.3	0.4318	0.37	0.2481	0.5648	-0.4964	9.5005	9.27834	9.10298	6.51793	6.36713
[illegible]	COL14A1	-2.5509	-3.1382	-2.5453	-2.5872	-1.5489	-4.4247	-1.3529	-1.7264	#	41	193.4	323.3	0.2431	0.5714	0.1327	0.7367	0.44218	9.25544	9.22655	8.06427	6.02362	4.90054
[illegible]	COL16A1	-4.288	-3.5232	-2.7285	-2.5963	-1.9309	-0.2837	-0.1338	-1.4574	#	20	158.2	323.3	2.1246	0.0075	0.9566	0.1105	2.33251	9.85148	9.84082	8.23606	6.6608	5.07762
[illegible]	COL1A1	-0.7449	-1.0639	-0.5439	-2.1609	-1.7163	-3.1441	-0.4799	0.9148	#	39	140.9	323.3	0.0079	0.982	0	1	0.02202	9.65377	9.63437	8.29414	6.46922	5.44235
[illegible]	COL1A2	-0.2977	-1.7969	-1.7827	-0.5529	0.20824	-0.735	-1.9893	-0.5437	#	43	104.4	323.3	0.2279	0.5916	0.1329	0.7363	0.34263	8.86926	8.8569	7.31714	5.26689	3.80061
[illegible]	COL2A1	-2.7596	-2.8606	-3.025	-3.4285	-3.8645	-2.7897	-3.6147	-3.1441	#	72	141.7	323.3	0.554	0.2792	0.3207	0.4778	-0.3348	12.0086	11.9943	10.4912	9.22819	7.88981

[illegible]